Science of the Total Environment 628–629 (2018) 1058–1078

Contents lists available at ScienceDirect

Science of the Total Environment

journal homepage: www.elsevier.com/locate/scitotenv

Influence of moisture source dynamics and weather patterns on stable isotopes ratios of precipitation in Central-Eastern Africa

Charles M. Balagizi [a,*], Marcellin M. Kasereka [a], Emilio Cuoco [b], Marcello Liotta [c]

[a] Geochemistry and Environmental Department, Goma Volcano Observatory, 142, Av. du Rond-point, Goma, Democratic Republic of the Congo
[b] Università della Campania "Luigi Vanvitelli", Via Vivaldi 43, 81100 Caserta, Italy
[c] Istituto Nazionale di Geofisica e Vulcanologia, Sezione di Palermo, Via Ugo La Malfa, 153, 90146 Palermo, Italy

HIGHLIGHTS

- We report the first δ^2H and $\delta^{18}O$ of precipitation of the Virunga, Central-Eastern Africa.
- δ^2H and $\delta^{18}O$ of precipitation show clear seasonality controlled by the season variation.
- Moisture from soil-plants predominates in wet seasons and that from lakes in the dry season.
- δ^2H and $\delta^{18}O$ of precipitation are typical of high altitude recycled continental moisture.
- δ^2H and $\delta^{18}O$ of precipitation are intermediate between that from Central and East Africa.

GRAPHICAL ABSTRACT

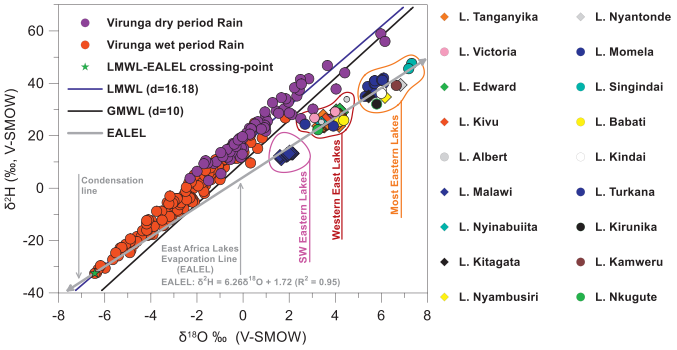

ARTICLE INFO

Article history:
Received 18 October 2017
Received in revised form 9 January 2018
Accepted 28 January 2018
Available online 20 February 2018

Editor: R Ludwig

Keywords:
Virunga precipitation stable isotopes
Moisture source for Virunga
Virunga precipitation variability
East African Lakes stable isotopes
Virunga Local Meteoric Water Line

ABSTRACT

We report the first $\delta^{18}O$ and δ^2H data of Virunga rainfall in the Eastern Democratic Republic of the Congo, situated on the limit between Central and Eastern Africa. The dataset is from 13 rain gauges deployed at Mount Nyiragongo and its surroundings sampled monthly between December 2013 and October 2015. The $\delta^{18}O$ and δ^2H vary from −6.44 to 6.16‰, and −32.53 to 58.89‰ respectively, and allowed us to define a LMWL of $\delta^2H = 7.60\delta^{18}O + 16.18$. Three main wind directions, i.e. NE, E and SE, were identified in the upper atmosphere corresponding to three major moisture source regions. On the contrary, lower atmospheric winds are weaker in nature and originate mainly from the S and SW, creating a topographically-driven, more local moisture regime. The latter is due to the accumulation in the floor of the rift of water vapor from Lake Kivu forming a layer of isotopically enriched vapor that mediates the isotope enrichment of the falling raindrops. A strong seasonality is observed in both $\delta^{18}O$ and δ^2H data, and is primarily driven by combined seasonal and spatial variation in the moisture sources. The $\delta^{18}O$ and δ^2H seasonality is thus correlated to weather patterns, as the latter control the wet to dry season shifting, and vice versa. The key characteristic of seasonality is the variation of monthly precipitation amounts, since the mean monthly air temperature is nearly constant on an annual scale. Two regionally relevant hydrological processes contribute to the isotopic signature: namely moisture uptake from the isotopically enriched surface waters of East African lakes and from the depleted soil-water and plants. Consequently, the proportion of water vapor from each of these reservoirs in the atmosphere drives the enrichment or depletion of δ^2H and $\delta^{18}O$ in the precipitation. Thus, during wet periods the vapor from soil-plants evapotranspiration dominates yielding isotopically depleted precipitation, contrary to dry periods when vapor from lakes surface evaporation dominates, yielding isotopically enriched precipitation. At the global scale, our dataset reduces gaps in this region that has been poorly studied for $\delta^{18}O$ and δ^2H in precipitation. At the regional scale, the improved understanding

* Corresponding author.
E-mail address: balagizi.charles@gmail.com (C.M. Balagizi).

https://doi.org/10.1016/j.scitotenv.2018.01.284
0048-9697/© 2018 Elsevier B.V. All rights reserved.

of the ways land cover, moisture source seasonal and spatial dynamics, and atmospheric patterns impact precipitation spatial and temporal variabilities in Central-East African will contribute to the ongoing research on mitigating the impacts of ongoing climate change in Sub-Saharan Africa. The reduction of gaps and uncertainties in δ^2H and $\delta^{18}O$ of precipitation, and the understanding of their interrelation with weather patterns are essential for a better past, present and future environmental and climatic modelling at both local and regional scales.
© 2018 Elsevier B.V. All rights reserved.

1. Introduction

Meteorological conditions are the key drivers for precipitation spatiotemporal variabilities as they govern water vapor formation, moisture transportation and later the formation of clouds and rainfall. In addition, land-forms, -cover, and -use may also greatly impact precipitation spatial and temporal variability at the regional scale (Pielke et al., 2007; Mahmood et al., 2014). The changes in the global and regional land cover and use, principally as a consequence of anthropogenic activities, have played a significant role in the ongoing global climate change (Singh and Shi, 2014; Mutiibwa et al., 2014). The latter have yielded perturbations in the rainfall regimes (Zeng et al., 1999; Feng et al., 2013; Zhang et al., 2015) and impacts natural ecosystems and human health (e.g. Patz et al., 2005; Piao et al., 2010; Brawn et al., 2017).

Sub-Saharan Africa is one of the most physically vulnerable places to the repercussions of climate change (Kotir, 2011; IPCC, 2014). Yet, in addition to the increase in drought events and the expansion of desertification (Reich et al., 2001; Eriksen, 2001; Lindsay et al., 2009), climate change has induced perturbations in the Sub-Saharan rainfall regime and caused an increase in the number of extreme weather events (Barasa et al., 2013; Niang et al., 2014; Egeru et al., 2014). Sub-Saharan African agriculture is also strongly threatened by the climate change because of its direct dependence on rainfall; many impacts have been noted so far. These impacts include food scarcity, leading to an increase of the prices of agricultural products and several mass movements of the populations (FAO, 2016). The ongoing fast rates of the East African human population (UNPD, 2015; Seto et al., 2012; Boke-Olén et al., 2017) will undeniably be accompanied by an increase in the demand for agricultural lands. This is expected to yield substantial deforestation over the coming decades (Akkermans et al., 2014; DeFries et al., 2010), making the above described repercussions of climate change even more significant for this region.

In the last few decades, several studies have focused on assessing the repercussions of climate change in Sub-Saharan Africa (e.g. Patz et al., 2005; Lobell et al., 2008; Mendelsohn, 2008; Serdeczny et al., 2016) and/or model future impacts (e.g. Kotir, 2011; Akkermans et al., 2014; Müller et al., 2014; Chadwick et al., 2016). Others attempted to develop strategies for adaptation or reducing the vulnerability to climate change (e.g. Sultan and Gaetani, 2016; Tabbo et al., 2016; Hassen et al., 2017). Numerical predictions of climate in Sub-Saharan Africa are necessary to better assess climate change processes; to prepare strategies to prevent the impacts, and to provide improved support for policy changes. Ground-based observations are indispensable for such numerical predictions to improve the understanding of the interactions between the atmosphere, the terrestrial ecosystem and the regional hydrology. Recorded terrestrial proxies (e.g. bivalve shells; Kelemen et al., 2017) and their link to hydrological and meteorological conditions provide important constraints on the effects of local and more remote processes on precipitation spatial and seasonal variations, and therefore, to potentially forecast perturbations in regular precipitation cycle.

Rainwater stable isotopes ratios (i.e. $\delta^{18}O$ and δ^2H) have been used to address problems related to the precipitation cycle, including tracing the water vapor source, moisture transportation, and precipitation formation (e.g. Gat, 2010; Aggarwal et al., 2016; Wirmvem et al., 2016; Putman et al., 2017). This tool provides valuable information about the role played by the land and atmospheric conditions on precipitation spatial and temporal variability. The weighted mean excess in deuterium is dependent on the fractionation physical conditions during water vapor formation at the source region (Merlivat and Jouzel, 1979; Johnsen et al., 1989; Pfahl and Wernli, 2008). Some successive rain events may thus show different $\delta^{18}O$ and δ^2H values because they are both meteorologically and seasonally dependent (Gat and Tzur, 1967). The $\delta^{18}O$ and δ^2H data points from worldwide precipitation show a relationship of $\delta^2H = 8\delta^{18}O + 10$, known as the Global Meteoric Water Line (GMWL) (Craig, 1961; Rozanski et al., 1993). The deuterium excess (d-excess) has application in climatic studies for reconstructing past and tracing present precipitation processes as it is correlated with the physical conditions under which the rain forms, i.e. the Relative Humidity (RH), air temperature and sea surface temperature (Gat and Carmi, 1970; Merlivat and Jouzel, 1979; Froehlich et al., 2002; Gat et al., 2003). The information provided by the isotopic composition of precipitation, i.e. regional meteorological conditions, vapor source physical conditions, atmospheric circulation pattern, and on large extent land form and cover (e.g. Pereira et al., 2014 and Wang et al., 2017 for Amazon); can therefore contribute to mitigating the climate change.

The main purpose of this study is to determine the $\delta^{18}O$ and δ^2H ratios of precipitation at Mount Nyiragongo and its surroundings and Lake Kivu surface water in the Virunga, an area situated in the transition zone between Central and Eastern Africa (Fig. 1). Using the isotopic composition of precipitation and Lake Kivu surface waters, meteorological and hydrological data, and the land form and cover information, the paper also aims to show how these parameters are interrelated and govern the precipitation spatial and temporal variability at regional scale. Despite its regional and global climate importance, the Central and Eastern Africa regions, particularly the Democratic Republic of Congo (DRC), remain poorly investigated for $\delta^{18}O$ and δ^2H assessment in precipitation. Thus, the present study reduces gaps and uncertainties in the estimation of global temporal and spatial variations of $\delta^{18}O$ and δ^2H, the latter being useful for better past, present and future environmental and climatic modelling.

2. Material and methods

2.1. Study area geographical and climatic settings

Nyiragongo (1.52S, 29.25E; 3470 m a.s.l) is a volcano located in the eastern DRC near the border with Rwanda (Fig. 1). Nyiragongo and its neighboring Nyamulagira (3058 m a.s.l) are very active volcanoes, and the only presently active of the Virunga volcanic chain, which consists of eight major volcanoes (see compilation in Coppola et al., 2016; Bobrowski et al., 2016 and Balagizi et al., 2016a). The chain of mountains (peak at Mount Karisimbi, 4508 m a.s.l) is located along the borders between the DRC, Rwanda and Uganda, forms an EW-oriented alignment perpendicular to the Western Branch of the East African Rift System (EARS, Fig. 1). The Virunga Mountains and the rift edges mark an abrupt break in the topography, and delimit the Nile River basin to the N and E from that of the Congo River to the S and E (Fig. 2A). The mountain range also influences the circulation of regional winds, particularly those of the lower atmosphere. The hydrography of the Virunga consists of Lake Kivu (1460 m a.s.l.) to the south, which belongs to the Congo River basin; and Lake Edward (912 m a.s.l.) to the north in the Nile basin, each fed by hundreds of tributaries (Balagizi et al., 2015; Fig.

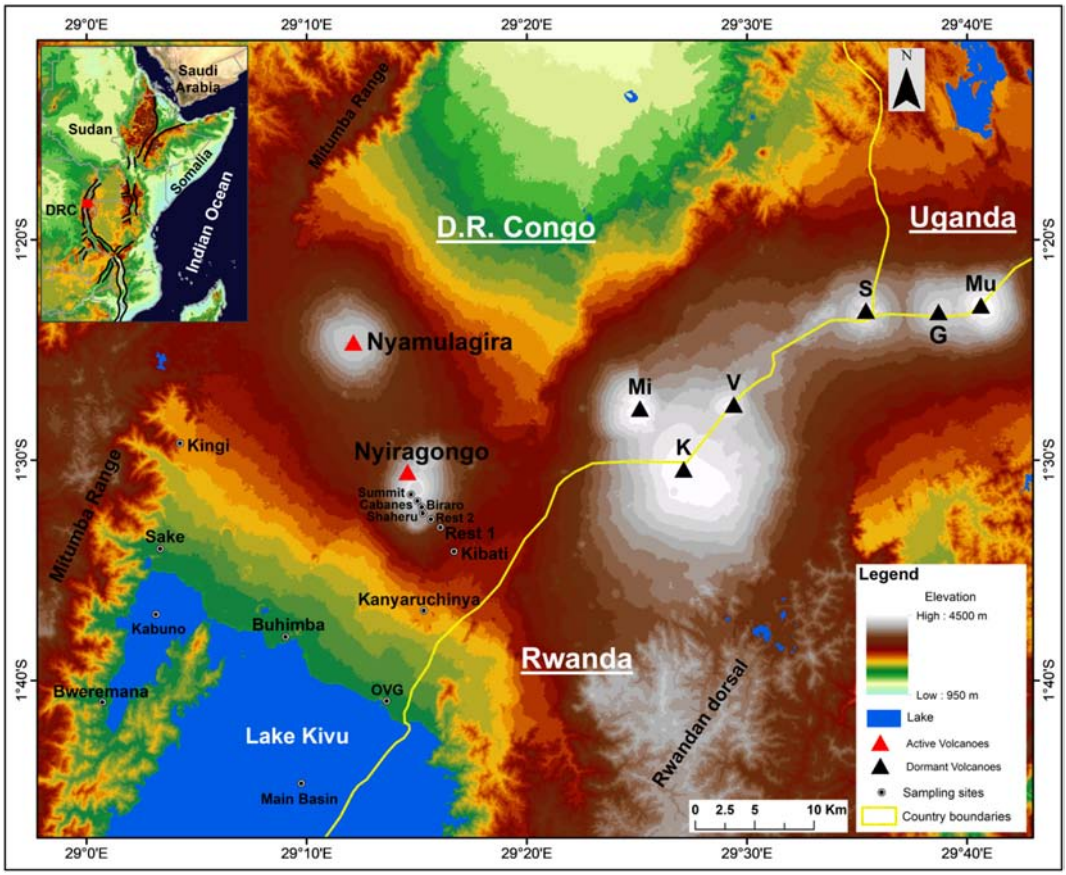

Fig. 1. Topographic map of the study area situated within the western branch of the East African Rift System (shown in the inset map). The sampling sites along the southern flank of Mt. Nyiragongo are in the following order, from farthest south to the volcano's summit: Kibati (1994 m above sea level, m a.s.l.), Rest 1 (2254 m a.s.l.), Rest 2 (2535 m a.s.l.), Shaheru (2761 m a.s.l.), Biraro (2918 m a.s.l.), Cabanes (3230 m a.s.l.) and Summit (3460 m a.s.l.). The Virunga chain of mountains are oriented EW and perpendicular to the axis of the Western Branch, and include Mt. Nyamulagira (3058 m a.s.l), Mt. Nyiragongo (3470 m a.s.l), Mt. Mikeno (Mi, 4437 m a.s.l), Mt. Karisimbi (K, 4508 m a.s.l), Mt. Visoke (V, 3911 m a.s.l), Mt. Sabinyo (S, 3647 m a.s.l), Mt. Gahinga (G, 3474 m a.s.l), and Mt. Muhabura (Mu, 4127 m a.s.l).

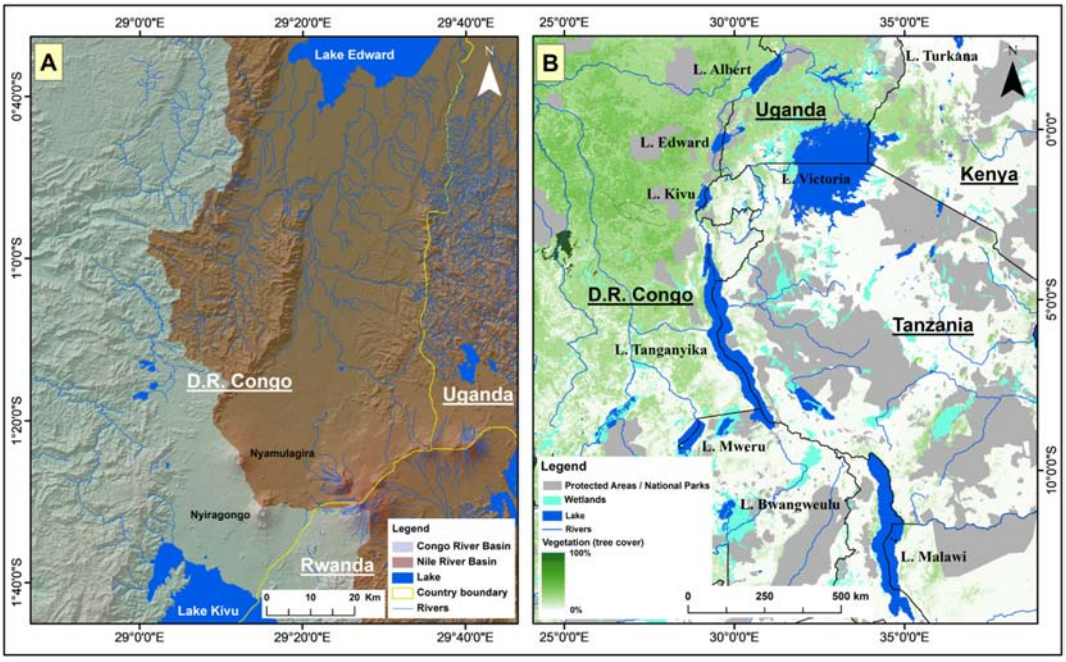

Fig. 2. The map (A) shows the hydrography of the Virunga region, while (B) shows the vegetation cover (as tree cover, ISCGM et al., 2008), protected areas (principally national parks, IUCN and UNEP-WCMC, 2015), and major rivers, lakes and wetlands (Lehner and Döll, 2004) of the African Great Lake region. Map (A) also shows the Congo and Nile Rivers basins limit all along the Virunga mountains chain and the rift edge.

2A). The Virunga is part of the African Great Lake Region (Fig. 2B) where the great lakes such as Victoria (water surface of 68,800 km^2; 1135 m a.s.l.), Tanganyika (32,900 km^2, 773 m a.s.l.), or Malawi (29,600 km^2; 474 m a.s.l) greatly impact the East African regional climate. The lakes are subject to important evaporation, e.g. ~1500 mm yr^{-1} for Lake Kivu (Muvundja et al., 2014), 1500–1750 mm yr^{-1} for Lake Victoria (Yin and Nicholson, 1998; Nicholson and Yin, 2001; Swenson and Wahr, 2009), 1700–2000 mm yr^{-1} for Lake Tanganyika (Bultot, 1993; Verburg and Hecky, 2003) and 1600–1800 mm yr^{-1} for Lake Malawi (Kidd, 1983; Mandeville and Batchelor, 1990; Lyons et al., 2011). Most East African lakes lose more water through evaporation than they receive from precipitation over their surface (see compilation in Shahin, 2013). Furthermore, Verburg et al., 2003 and Taylor et al., 2006 expect an increase of evaporation and evapotranspiration in the East African region as a response to global warming. Hence, the lakes play an important role in the regulation of the East African climate (Thiery et al., 2015), and thus impact on atmospheric dynamics and the regional hydrological cycle.

The combined effects of the Virunga mountains and the equatorial forest induce a local mountainous micro-climate at the Virunga highlands (Balagizi et al., 2015), even though a humid climate dominates at regional scale. Despite the human pressure on the forest and other ecosystems (Kolding et al., 2014), there generally still exist large forested zones mainly due to the presence of several protected areas and National Parks (Fig. 2B). The mean annual precipitation varies between 1300 and 1700 mm yr^{-1} at Virunga lowland areas (i.e. <2000 m a.s.l., Muvundja et al., 2014; Balagizi et al., 2017), but can reach up to 2300 mm yr^{-1} at highland localities situated above 2000 m a.s.l. (Balagizi et al., 2017). The Virunga precipitation regime is largely bimodal, with a dry season extending from July to August and the wet season spanning from September to June. There is however a secondary-like dry period observed in part of January and that of February. Since a few years, increasing perturbations in the timing of the seasons (i.e. beginning, end or their duration) have been observed in East Africa, as well as decreasing trends in rainfall (e.g. Nsubuga et al., 2014) and a decline in the long rains (e.g. Lyon and DeWitt, 2012). Monthly mean air temperature for a given location show little variation due to the proximity to the equator. However, the mean monthly and annual temperature show great disparities between lowlands (~20 °C, with daily maxima up to 32 °C) and highlands (~10 °C, with daily minima down to 7 °C) (Balagizi et al., 2017).

2.2. Remote data acquisition

The GIS layers of the surface rivers of the Virunga region (Fig. 2A) were generated using a SRTM DEM data sampled at 3 arc *sec* (~30 m) pixel size computed using the HydroSHEDS mapping product (Lehner et al., 2006). The same SRTM DEM was used to generate the topographical map of the sampling site shown in Fig. 1. The description of the SRTM DEM data collection and reanalysis can be found in Farr et al., 2007 and Zandbergen, 2008. In Fig. 2B, the dataset for vegetation cover as tree cover and the lakes is from ISCGM et al., 2008; the protected areas that include National Parks were extracted from IUCN and UNEP-WCMC, 2015, while the wetlands and the hydrography of major rivers of East Africa were obtained from the Global Lakes and Wetlands Database, Level 3 (GLWD) accessible at (www.worldwildlife.org/pages/global-lakes-and-wetlands-database) and described in Lehner and Döll (2004).

The air temperature, RH, wind speed and direction at the summit of Mt. Nyiragongo were obtained from the European Centre for Medium-Range Weather Forecasts (ECMWF, Kobayashi et al., 2009; Simmons et al., 2010; and Dee et al., 2011). The ERA-Interim model of the ECMWF provides daily dataset collected with 6 h interval, i.e. 6 and 12 AM, 6 and 12 PM, at a resolution of 0.25 × 0.25 degree. These meteorological data were used for the sites located on Mt. Nyiragongo where weather stations could not be installed because of field constraints, mainly the security of the equipment. For the other sites, meteorological data were collected using a Davis Vantage Pro2 weather station installed at OVG site shown in Fig. 1. However, the monthly and annual precipitation for all the sites were obtained from the volume of rainwater collected in the rain-gauges.

The moisture source region that generated the rainfall in the study area was computed using the Backward Trajectories Model database, which is based on the Hybrid Single-Particle Lagrangian Integrated Trajectories model (HYSPLIT) (https://ready.arl.noaa.gov/hypub-bin/trajtype.pl?runtype=archive). The HYSPLIT calculation method is a combination between a moving frame of reference that follows air parcels as they move from their initial location for the simulation of advection, diffusion, and deposition (Lagrangian) and a fixed three-dimensional grid as a frame of reference (Eulerian) (Stein et al., 2015; Rolph et al., 2017). The used frequency option of the HYSPLIT starts a trajectory from a single location (here the summit of Mt. Nyiragongo) and height (1000 m above ground) every 12 h with total run time of 48 h, and then sums the number of times the trajectories pass over each grid cell of 1.00 × 1.00 degree resolution. We thus calculated monthly backward trajectories (number of days to calculate trajectory frequencies = 30 days) for the period from December 2013 to October 2015, which allowed for the identification of the changes in the moisture source regions that produced the rains falling over the study area.

Monthly Potential Evapotranspiration (PET) and soil-water content for the African Great Lakes region were obtained from the Global-Potential Evapotranspiration and Global-Soil-Water Balance databases respectively (Trabucco and Zomer, 2009). The reported PET is a measure of the ability of the atmosphere to remove water through evapotranspiration processes (Allen et al., 1998). The Global PET was modeled using the WorldClim global climate data (http://WorldClim.org) as input parameters (Hijmans et al., 2004). The latter is composed of monthly average climate observations (e.g. precipitation, mean, minimum and maximum temperature) from 1950 to 2000. The soil water content is derived from a Global high-resolution Soil-Water Balance dataset and provides hydrological raster data with a resolution of 30 arc *sec* (~ 1 k m at the equator). This soil-water balance utilizes both WorldClim and Global-PET as primary inputs data. The methods used to derive these datasets and the data dictionary are further discussed in Trabucco et al. (2008) and Zomer et al. (2007, 2008).

2.3. Sample collection and analytical methods

Monthly samples were collected from 13 rain gauges installed at different altitudes of Mt. Nyiragongo and its surroundings (Fig. 1), and were sampled from December 2013 to October 2015. Each precipitation collector consisted of a circular plastic funnel of 247.58 mm diameter fixed on a 30 L plastic container in which 250 mL of pure Vaseline oil was added to avoid evaporation processes. Samples were collected at the end of each month: after measuring the amount of water collected, the required aliquot of water for laboratory analyses was taken and the collector emptied and thoroughly washed with distilled water. The monthly precipitation amount was obtained by dividing the collected volume of water over the surface of the funnel. The containers were changed every 2–3 months during the study period. Throughout the course of the study, additional samples were collected from the surface water and the upper seasonally mixed layer of the meromictic Lake Kivu (Fig. 1). Three campaigns were thus conducted in Kabuno Bay (Fig. 1, on December 7, 2013; February 9, 2014 and February 13, 2015), and two others in the Main Basin of Lake Kivu on February 28, 2014 and February 7, 2015. Water samples were taken from depths (from 5 and 10 m in Kabuno Bay; and 25 m depth in the Main Basin) and the surface of both basins using a 5 L Niskin bottle (Ocean Scientific International Ltd., OSIL- United Kingdom). Both rain and lake water samples were filtered in the field though 0.45-mm-pore-size polysulfone syringe filters and stored at room temperature in 30 mL high-density polyethylene plastic bottles with double screwcaps. The filtration was needed to

Table 1
Site elevation (meter, m), monthly min-mean-max air relative humidity (percentage saturation, %), monthly min-mean-max air temperature (centigrade degrees, °C), monthly min-mean-max precipitation (millimetre, mm), monthly min-arithmetic mean-max δ^2H and $\delta^{18}O$ (per mil), and mean precipitation weighted values of rainwater collected on a monthly basis at Mount Nyiragongo and its surroundings, Democratic Republic of the Congo, between December 2013 and October 2015.

	Elevation (m a.s.l.)	Relative Humidity[a] (%)			Temperature[a] (°C)			Precipitation[b] (mm)			δ^2H (‰)			$\delta^{18}O$ (‰)			d-excess (‰)			Mean precipitation weighted values		Number of samples
		Min	Mean	Max	Min	Mean	Max	Min	Mean	Max	Min	Mean	Max	Min	Mean	Max	Min	Mean	Max	δ^2H (‰)	$\delta^{18}O$ (‰)	d (‰)	
Bweremana	1470							9.87	110.80	218.11	−12.22	10.84	58.89	−3.42	−0.27	5.98	−3.58	13.02	20.20	5.45	−1.07	14.03	23
Sake	1514							4.26	107.49	206.47	−18.10	8.95	41.74	−4.15	−0.81	4.04	5.54	15.40	19.69	3.28	−1.51	15.38	23
Kingi	1848							14.12	139.45	283.12	−17.91	3.30	29.46	−4.22	−1.62	1.44	13.42	16.25	19.20	0.31	−1.99	16.27	18
Buhimba	1468							5.71	119.87	223.61	−21.47	7.10	37.44	−4.74	−1.17	2.44	11.11	16.49	20.49	2.93	−1.65	16.16	20
OVG	1535	32.00	78.37	99.00	13.60	21.02	32.40	7.27	104.51	214.78	−17.73	4.54	32.87	−3.99	−1.38	2.51	6.47	15.54	20.37	−0.74	−2.09	16.01	21
Kanyaruchinya	1759							7.48	139.32	320.30	−18.47	8.91	56.02	−4.60	−0.89	6.16	6.74	16.00	22.03	4.03	−1.53	16.23	22
Kibati	1994							5.40	143.74	263.80	−23.70	5.29	34.11	−4.87	−1.41	1.86	11.24	16.60	19.48	2.57	−1.73	16.40	22
Rest 1	2254							12.05	194.11	372.44	−24.61	4.41	46.80	−4.91	−1.63	3.66	14.69	17.42	20.82	0.27	−2.12	17.24	14
Rest 2	2535							15.37	188.31	376.60	−25.84	0.90	41.50	−5.42	−2.19	2.49	15.92	18.40	21.58	−3.39	−2.69	18.16	14
Shaheru	2761							53.18	176.36	339.21	−27.27	2.99	39.75	−5.66	−2.01	2.53	17.41	19.08	20.86	−0.47	−2.41	18.78	12
Biraro	2918							35.73	194.35	357.28	−30.54	−2.02	34.51	−5.99	−2.76	1.66	17.37	20.06	21.83	−6.71	−3.31	19.78	12
Cabanes	3230							47.98	177.01	339.00	−32.30	−3.73	29.08	−6.36	−3.01	0.95	18.56	20.38	23.48	−7.66	−3.47	20.07	12
Summit	3460	32.94	78.98	104.64	7.16	9.64	13.68	23.26	174.60	274.40	−32.53	−7.19	32.64	−6.44	−3.50	1.28	18.74	20.78	22.92	−11.66	−4.00	20.36	10

[a] Relative humidity and air temperature data for OVG (in Goma city) are from a ground-based weather station, while that for Nyiragongo summit are from remote measurements by the ECMWF (European Centre for Medium-Range Weather Forecasts) model.
[b] Precipitation is deduced from the volume of monthly rainwater recorded in the rain-gauge for each station.

remove suspended materials in both rain and Lake Kivu water samples, and traces of Vaseline oil in rainwater samples. No preservatives were added to the samples. The configuration of the stations allowed us to capture any altitudinal variations of $\delta^{18}O$ and δ^2H, whereas the sampling campaign that lasted 23 months and covered each of the 2 seasons twice allowed us to capture the seasonal variations. Due to security constraints, we were not able to access 6 sites of Mt. Nyiragongo (from Rest 1 to summit, refer to Fig. 1) for the period between January and October 2014 because this zone was occupied by armed rebel groups.

Hydrogen and oxygen stable isotopes analysis were conducted in the Isotope Hydrology Laboratory of the International Atomic Energy Agency (IAEA) in Vienna. The analyses were performed using an off-axis integrated cavity output laser spectroscopy (OA-ICOS), following analytical procedure of Wassenaar et al. (2014). Samples were run in duplicate on a different day and instrument. Samples for which repeatability of the two runs was not within 2 times the typical uncertainty (see below) were repeated on a dual-inlet isotope ratio mass spectrometer (Isoprime DI 100) following equilibration with H_2 or CO_2 gases respectively (Epstein and Mayeda, 1953; Coplen et al., 1991). A few samples were analyzed at the Istituto Nazionale di Geofisica e Vulcanologia (INGV) in Palermo using Analytical Precision AP 2003 and Finnigan MAT Delta Plus spectrometers to analyze $\delta^{18}O$ and δ^2H, respectively. The $\delta^{18}O$ and δ^2H are reported as per-mille (‰) deviation relative to the Vienna-Standard Mean Ocean Water (V-SMOW). The d-excess was deduced from Dansgaard's equation relating the $\delta^{18}O$ and δ^2H of water, by the relation $d = \delta^2H\text{-}8\delta^{18}O$ (Dansgaard, 1964). The typical uncertainty is reported as the long-term standard-deviation of a dedicated control sample and amounts to 0.08‰ for $\delta^{18}O$ and 0.50‰ for δ^2H.

The mean vertical δ^2H, $\delta^{18}O$ and d-excess gradients (given per 100 m; i.e. δ^2H/100 m, $\delta^{18}O$/100 m and d/100 m) were computed as follows:

$$\delta^2H\ (‰) = \frac{\Delta\delta^2H \text{ x } 100}{\Delta z};$$

$$\delta^{18}O(‰) = \frac{\Delta\delta^{18}O \text{ x } 100}{\Delta z}, \text{and}$$

$$d(‰) = \frac{\Delta d \text{ x } 100}{\Delta z}$$

where $\Delta\delta^2H$, $\Delta\delta^{18}O$ and Δd denote the difference between δ^2H, $\delta^{18}O$ and d-excess values at higher and lower elevated sites respectively, and Δz the elevation (z) difference. The δ^2H and $\delta^{18}O$ values used in the above formula are mean precipitation-weighted values (δ_{pw}) calculated as given below:

$$\delta_{pw} = \frac{\sum_{i=1}^{n} \delta_i \text{ x } P_i}{\sum_{i=1}^{n} P_i}$$

where δ_i represents the measured monthly δ^2H or $\delta^{18}O$ values, and P_i the monthly precipitation. The mean precipitation-weighted d-excess values were thereafter computed from the obtained δ^2H and $\delta^{18}O$ precipitation-weighted values.

Similarly, the $\delta^{18}O$ dependency on precipitation amounts (given per 100 mm of rainwater; $\delta^{18}O$/100 mm) was calculated following the equation:

$$\delta^{18}O(‰) = \frac{\Delta\delta^{18}O \text{ x } 100}{\Delta P};$$

where $\Delta\delta^{18}O$ and ΔP denote respectively the difference between the monthly higher and lower $\delta^{18}O$ values, and the recorded higher and lower monthly precipitation at a given station of the study area.

The relationship between δ^2H and $\delta^{18}O$ in local precipitation, defined as the Local Meteoric Water Line (LMWL), which is of the form $y = ax + b$ (where y and x refer to δ^2H and $\delta^{18}O$, respectively) was determined using the traditional Ordinary Least Squares Regression

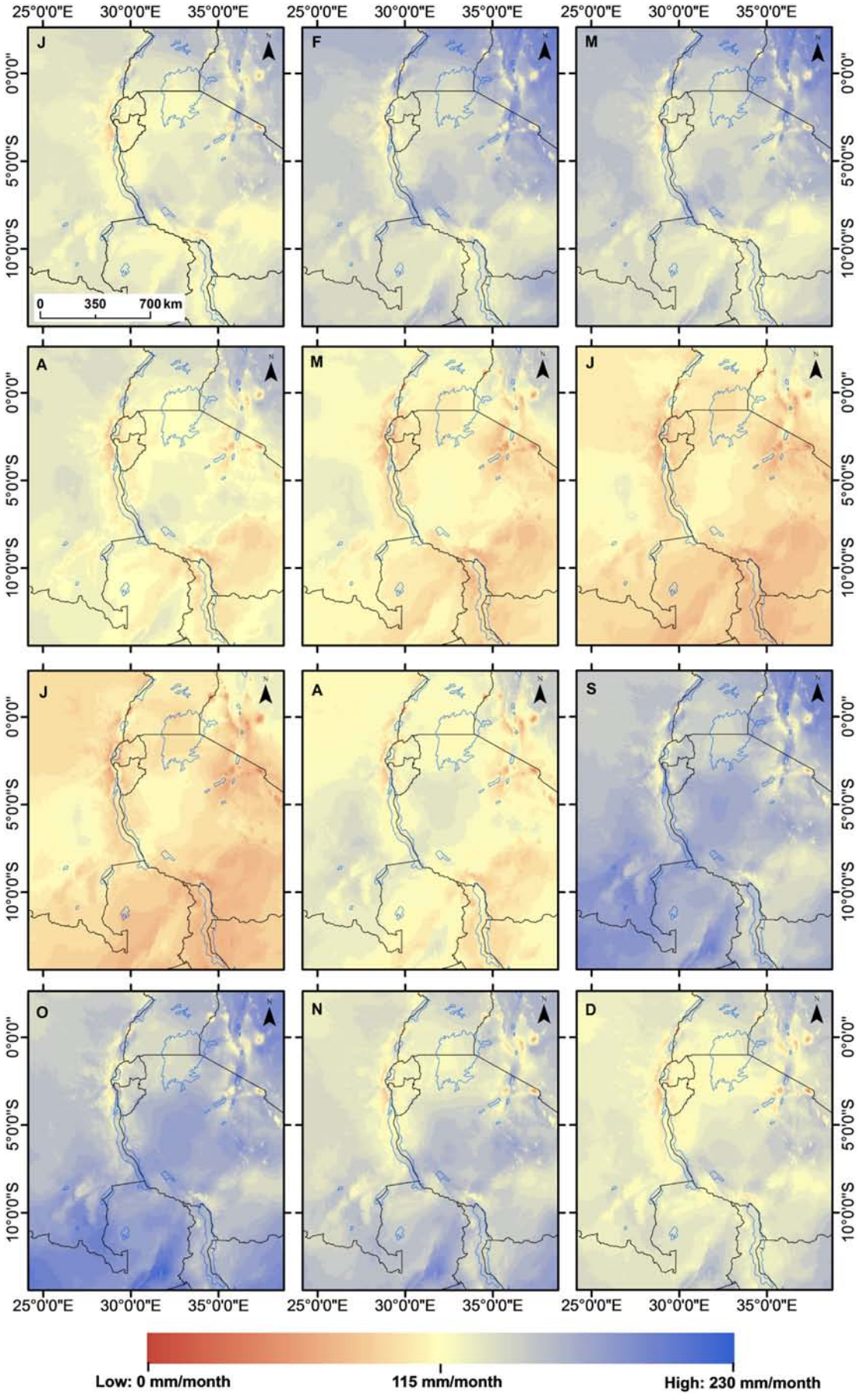
25°0'0"E
30°0'0"E
35°0'0"E
0°0'0"
5°0'0"S
10°0'0"S
J
F
M
A
M
J
J
A
S
O
N
D
0 350 700 km
Low: 0 mm/month
115 mm/month
High: 230 mm/month

(OLSR) analysis described in IAEA (1992). Additional LMWLs were determined by integrating the precipitation amounts in the calculations for the whole dataset, and the dry and wet periods. The integration of precipitation amounts is necessary as it reduces the effect of small precipitation samples on the calculations of the LMWL, and uses the Precipitation Weighted Least Squares Regression (PWLSR) method described in Hughes and Crawford (2012).

3. Results

3.1. Ground and remote meteorological data

The sampling sites spatial and basic statistical characteristics are reported in Table 1, the complete datasets are available in Dataset S1 and Dataset S2 supplementary materials. The sites located below 2000 m a.s.l. (i.e., Bweremana, Sake, Kingi, Buhimba, OVG, Kanyaruchinya and Kibati, hereafter referred to as the lowland sites) were characterized by higher air temperatures compared to those at the summit of Nyiragongo (Table 1). At Mt. Nyiragongo's summit, the daily temperature ranged from 7.2 to 13.7 °C, and the RH between 32.94 and 104.64%; while at OVG station the temperature ranged from 13.6 °C to 32.4 °C, and the RH from 67 to 99% (Dataset S2). For the year 2014, the mean annual temperature and RH at OVG were 22.2 °C and 78.7% respectively, and 9.5 °C and 80.2% at Nyiragongo summit. As a general trend, the lower mean monthly temperatures and RH were recorded during the dry season periods (Fig. S1, Dataset S2). The precipitation amounts followed opposite trends to that showed by the temperature, and hence the higher precipitations were recorded at highland sites found above 2000 m (Table 1).

The reported PET (Fig. 3) represents the sum of the potential quantity of water removed from the soil due to evaporation and from leaves through plant transpiration. The PET rate is affected by several factors such as wind, air temperature, atmospheric RH, and water availability (here as precipitation and soil-moisture); and varies accordingly with both space and season. Spatially the PET in the African Great Lakes region shows lower values at higher altitudes situated all along the edges of the EARS and at the summits of tall mountains (Fig. 3), e.g. the Mitumba range, the Virunga mountains, the Ruwenzori mountains (5109 m a.s.l.), Mount Kenya (5199 m a.s.l.), or Mount Kilimanjaro (5895 m a.s.l.). The low PET of these high altitude areas is in line with their low vegetation coverage (e.g. Bussmann, 2006; Hemp, 2009) and low air temperature (Diaz and Bradley, 1997; Christy et al., 2008; Duane et al., 2008; Balagizi et al., 2017) which lower the evapotranspiration process rates. On temporal basis, the PET varies with season, and showed maximum values during the wet season (Fig. 3) as consequence of the high precipitation and soil-moisture availability characterizing this season. Temporally the soil-water content shows similar trends as the PET, and therefore decreases with the decrease of precipitation (Fig. 4). Spatially the soil-water content showed the highest values at higher altitudes because of many factors such as the lower removal rates of soil-water at these areas due to their low air temperature, and given the fact that they receive high precipitation.

The wind rose charts of Fig. 5 display the wind speed and direction distribution at OVG station (A) and the summit of Mt. Nyiragongo (B), where consecutive months with common dominant wind direction are grouped. Three main wind directions have been identified on an annual scale at the summit: between December and March the wind blows from the NE, comes between the E and SE from April to July with a SE preference, while from August to November the *E*-SE warding origin is conserved but shows a preferential inclination towards the E (Fig. 5B). On the other hand, only 16% of the wind had speeds higher than 6.4 m s^{-1}, while ~35% showed speeds between 4 and 6 m s^{-1}, and the remaining ~49% had speeds <4 m s^{-1}. In Goma at OVG station, for the majority of the months, the winds do not show a predominant direction and are characterized with a lower speed (Fig. 5A) because Goma and the lowland sites are situated in the floor of the rift (Fig. 1). Nevertheless, between April and July the wind shows a clearly defined orientation and originates from the S-SW, with a weak inclination to the south. Circulating in the lower atmosphere, Goma's local wind is also of low speed (generally between 2 and 4 m s^{-1}) compared to the regional winds at the summit (Fig. 5A and Fig. S2–3) circulating in the upper atmosphere. The monthly wind speed and direction charts for the whole sampling period are given in Fig. S2 and Fig. S3 in the supplementary materials.

The moisture source follows similar dynamics as the regional winds, and hence three main moisture sources are noted corresponding to the NE, E and SE (Fig. 6). However, in the lower atmosphere there exists a permanent local moisture source point, which is due to the accumulation in the floor of the rift of water vapor evapotranspired from the neighboring Lake Kivu and its catchment. Fig. S4 in the supplementary materials shows in details the monthly moisture source dynamics for the study area.

3.2. Oxygen and hydrogen stable isotopes variations

The arithmetic mean, minimum and maximum δ^2H and $\delta^{18}O$ of monthly rainwater at Mt. Nyiragongo and its surroundings are given in Table 1. The full dataset for all sampling sites is available in Dataset S1 supplementary material. This study is the first $\delta^{18}O$ and δ^2H data to be reported for precipitation in the Virunga region and the Eastern DRC using regular monthly collection, even single precipitation events had never been reported. The highest and lowest values are either related to seasonal variation or to secondary effects that modify the pristine isotopic composition of rainwater (see later discussion). Based on site mean values, Bweremana (1470 m a.s.l.) and Nyiragongo summit (3460 m a.s.l.) appear as the two end members, the former showing the most enriched δ^2H and $\delta^{18}O$ mean values (10.84 and −0.27‰ respectively) and the latter the most depleted (−7.19 and −3.50‰, respectively for δ^2H and $\delta^{18}O$; Table 1). At local lowlands sites, the d-excess values at a given station show marked differences, for example it varies between −3.58‰ and 20.20‰ at Bweremana or 6.47‰ and 20.37‰ at OVG. On the contrary, the d-excess of the highland stations falls within a narrow range, e.g. it varies from 18.56 and 23.48 at Cabanes, and from 18.74 and 22.92 at the summit (Table 1, Dataset S1). As a general trend, the lower and higher d-excess are found during the dry and wet periods, respectively. The δ^2H and $\delta^{18}O$ of Lake Kivu surface water showed little temporal variation, and little variation with depth because they were all collected from the upper seasonal mixing layer (Table 2). However, the δ^2H and $\delta^{18}O$ of the surface waters of the main basin are almost twice heavier compared to Kabuno Bay, but the latter has the higher d-excess values.

4. Discussion

4.1. Local meteoric water line

For the first time, our data allowed us to define a LMWL for the Virunga region and the eastern DRC in general using 223 measurements of local rainwater. The monthly δ^2H and $\delta^{18}O$ values of Virunga precipitation were strongly correlated ($r^2 = 0.97$, $p < 0.0001$), and showed a best-fit line of equation $\delta^2H = (7.60 \pm 0.09)\ \delta^{18}O + (16.18 \pm 0.27$; OLSR method) which represents the LMWL (Fig. 7). A similar equation $\delta^2H = (7.89 \pm 0.09)\ \delta^{18}O + (16.89 \pm 0.27)$ ($R^2 = 0.97$) is obtained using the PWLSR method of Hughes and Crawford (2012). The most

Fig. 3. Monthly evapotranspiration for the African Great Lakes region extracted from the Global-Potential Evapotranspiration database after Zomer et al. (2007, 2008) and Trabucco and Zomer (2009). The scale for all the panels is similar as that for chart 1. The blue lines indicate lake shorelines, while the black indicate the country boundaries.

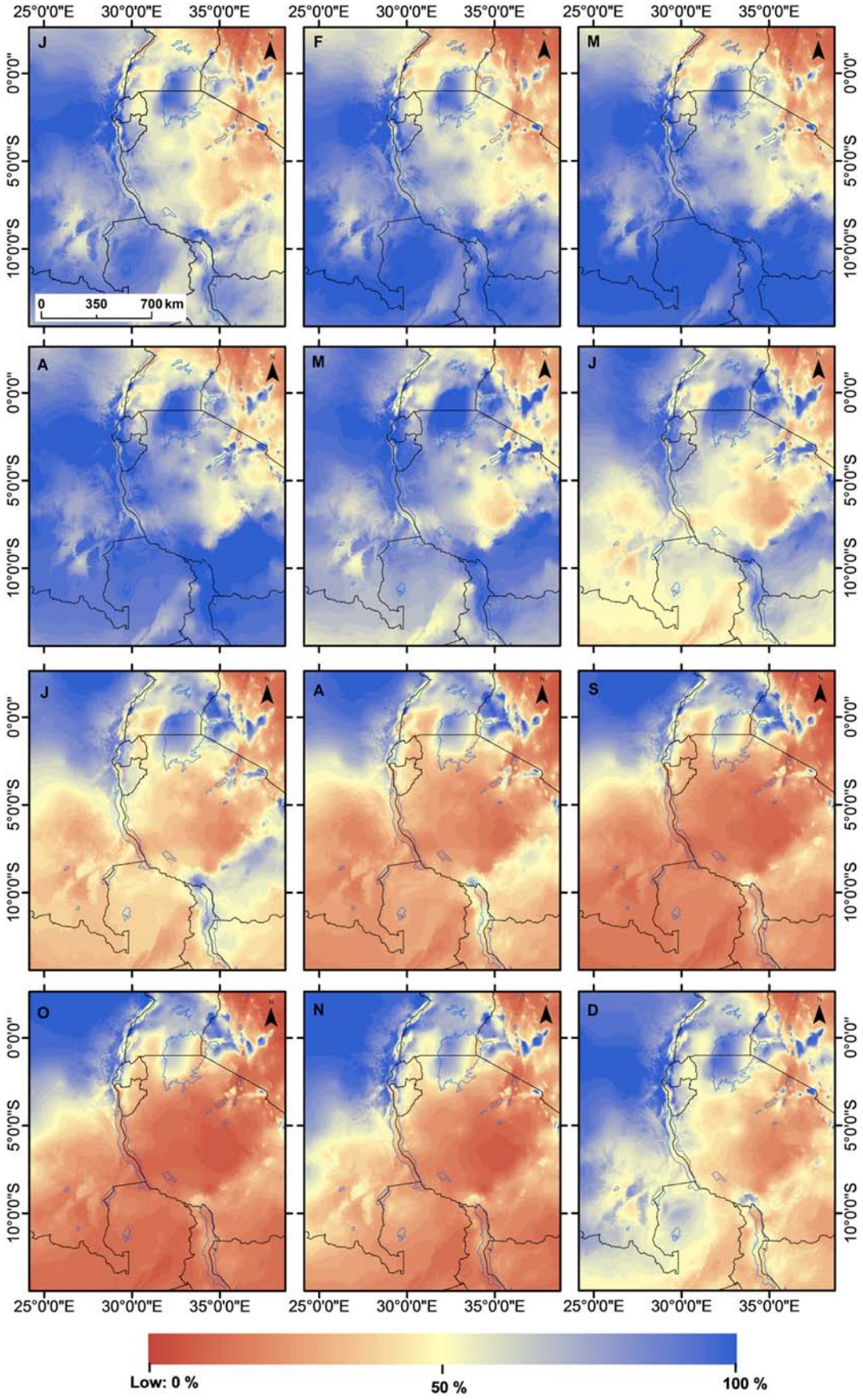

Fig. 4. Monthly soil-water content for the African Great Lakes region extracted from the Global-Soil-Water Balance database after Zomer et al. (2007, 2008) and Trabucco and Zomer, 2009. The scale for all panels is similar as that of chart 1. The blue lines indicate lake shorelines, while the black indicate the country boundaries.

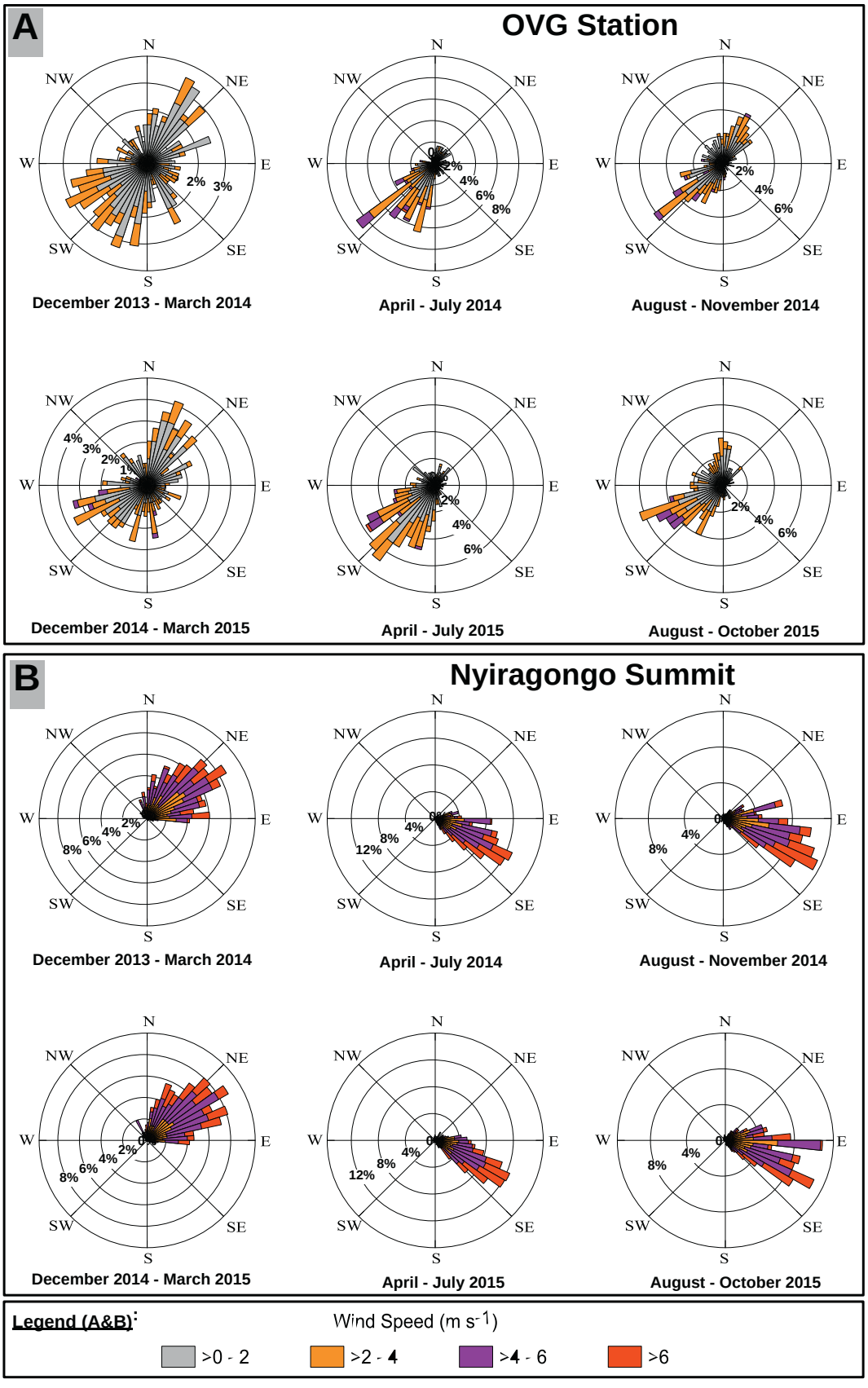

Fig. 5. Rose charts of annual main wind directions and speeds at OVG station (A) and the summit of Mt. Nyiragongo (B) (at 700 mbar) between December 2013 and October 2015. The grouped data were daily wind direction and speed collected on 6 h intervals by the ERA-Interim model of the European Centre for Medium-Range Weather Forecast (ECMWF).

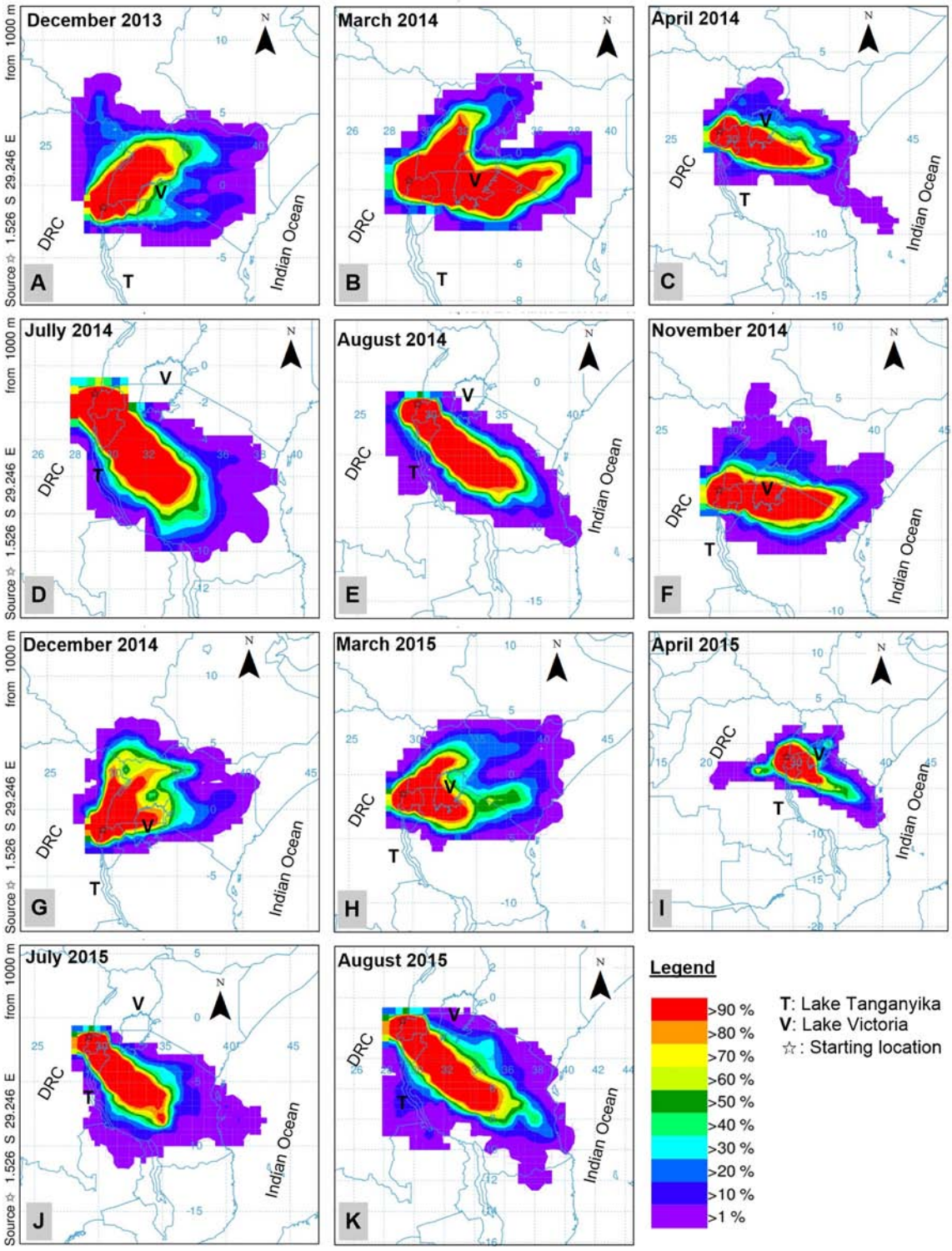

Fig. 6. Backward 48 h trajectory frequency plots from a starting location at the summit of Mount Nyiragongo (1.52S, 29.25E) indicated by the star in the charts. For each chart the contours represent, in percentage, the likely moisture source area that yielded the formation of precipitation at the starting location. On an annual scale time, the moisture source region changes as a result of the observed variation in wind direction.

enriched δ^2H and $\delta^{18}O$ are from samples collected at lowland sites (e.g. Bweremana, OVG or Buhimba) either during the January–February short dry season or the effective long dry season of July–August. These samples were further characterized by the lowest d-excess values (Dataset S1) at their respective sites, and showed an inclination towards the GMWL (Fig. 7). The low d-excess values characterizing the dry period could be related to the slight decrease in RH recorded during this period (e.g. Fig. S1), on the one hand. On the other hand, it could be a mark of a significant contribution from East African lakes water vapor to precipitation during the dry periods, which are characterized by low d-excess values (Table 3, Balagizi et al., 2016b). Water vapor from the lakes is in fact the major moisture source for the region during

Table 2
Stable oxygen and hydrogen stable isotopes ($\delta^{18}O$ and $\delta^{2}H$, expressed in per mil) of surface water and from the seasonally mixed layer of meromictic Lake Kivu, Democratic Republic of the Congo.

Basin	Depth (m)	Latitude (°)	Longitude (°)	Altitude (m a.s.l.)	Sampling date	$\delta^{2}H$ (‰)	$\delta^{18}O$ (‰)	d-excess (‰)
Kabuno Bay	0	−1.61	29.07	1460	07-12-2013	17.99	1.71	4.31
Kabuno Bay	5	−1.61	29.07	1460	07-12-2013	17.64	1.63	4.60
Kabuno Bay	0	−1.61	29.07	1460	09-02-2014	18.75	1.90	3.55
Kabuno Bay	5	−1.61	29.07	1460	09-02-2014	18.66	1.89	3.54
Kabuno Bay	0	−1.61	29.07	1460	13-02-2015	19.36	1.92	4.02
Kabuno Bay	10	−1.74	29.16	1460	13-02-2015	17.45	1.50	5.45
Kivu Main Basin	0	−1.74	29.16	1460	28-02-2014	26.22	3.58	−2.42
Kivu Main Basin	25	−1.74	29.16	1460	28-02-2014	26.05	3.63	−3.02
Kivu Main Basin	0	−1.74	29.16	1460	07-02-2015	27.76	3.41	0.50
Kivu Main Basin	25	−1.74	29.16	1460	07-02-2015	27.33	3.50	−0.63

the dry periods when the soil-plants evapotranspiration is brought to its minimal value (Fig. 3) (further discussed in Section 4.3.2.).

The Virunga LMWL has higher intercept (d = 16.18‰, Fig. 7) compared to the GMWL (d = 10‰, Craig, 1961) mainly due to the influence from samples collected at Virunga highland sites (some samples show d-excess values up to 23.48‰). However, the LMWL shows a slope of 7.6 which is comparable to the GMWL and reveals condensation processes near equilibrium conditions. The observed difference in d-excess between Virunga lowland and highland areas (e.g. mean of 13.02 at Bweremana versus 20.78‰ at the summit, Table 1) is typical of mountainous catchments showing a sudden to progressive topography change. Similar trends have been reported in other tropical climate regions, e.g. at Mt. Cameroon (e.g. Fontes and Olivry, 1976; Gonfiantini et al., 2001), and the Andes Mountains in the Ecuador (Windhorst et al., 2013); or in contrasting climate such as the Mediterranean, e.g. Mts Etna and Stromboli (D'Alessandro et al., 2004; Liotta et al., 2006a, 2006b, 2013). The Virunga LMWL has a slope comparable to that of Central African regions (Table 3), suggesting similar processes of rain formation during condensation (i.e. under equilibrium conditions) at the regional scale. This places the Virunga into the central African region; however the high intercept of the Virunga LMWL (Fig. 7, Table 1) and higher $\delta^{18}O$ values place the Virunga closer to the East Africa region.

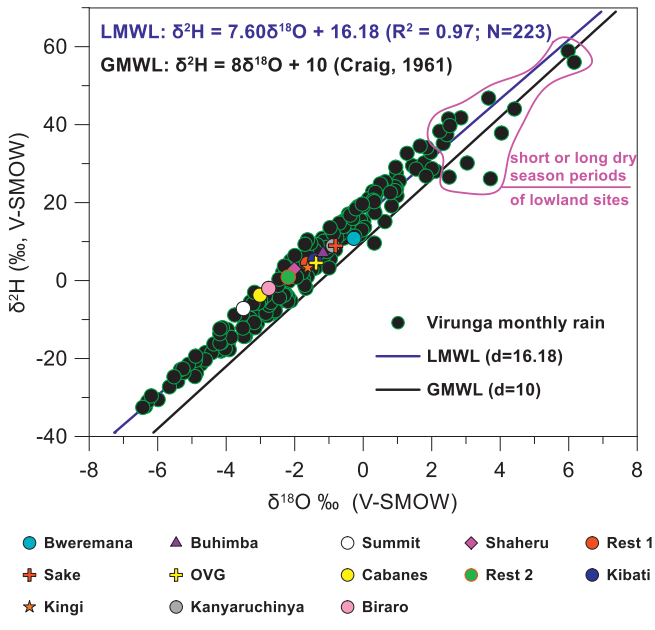

Fig. 7. Relationship between $\delta^{2}H$ and $\delta^{18}O$ in rainwater at Mt. Nyiragongo and its surroundings, Eastern Democratic of the Congo, between December 2013 and October 2015. The black dots are $\delta^{2}H$ and $\delta^{18}O$ monthly values, while the 13 dots of different symbols and colors represent the arithmetic mean values for each sampling site (corresponding legend is below the figure).

The high intercept of the Virunga precipitation LMWL are consistent with the high altitude origin of the recycled continental moisture arriving in the study area, while their enrichment in the heavy isotopes is related to the evaporative process at the source. For Cameroon, Central African Republic and the western DRC, in contrast, their lower intercepts (Table 3) are related to the low altitude continental moisture arriving in these regions compared to East Africa, or to direct water vapor from the Atlantic Ocean affecting some regions (e.g. Njitchoua et al., 1999).

4.2. Spatial variabilities in $\delta^{2}H$ and $\delta^{18}O$ and altitudinal gradient

Topographically-induced spatial variations of $\delta^{2}H$, $\delta^{18}O$ and d-excess are observed between the seven lower and six higher land sampling sites (Fig. 8). This is in line with the earlier noted classification of the sampling sites into two groups, the first being composed of local lowlands characterized with low slope and which are situated between ~1460 m of elevation (Lake Kivu level) and ~2000 m a.s.l. at Kibati (Fig. 1). Samples from this group were generally characterized by enriched $\delta^{2}H$ (mean from 3.30 to 10.84‰) and $\delta^{18}O$ (mean between −1.62 and −0.27‰) compared to the second group formed of highland sites (Fig. 8 and Table 1). These highland sites are located along the steep slope of Mt. Nyiragongo between ~2000 m a.s.l. and the summit (3470 m, Fig. 1), and showed depleted $\delta^{2}H$ (mean between −7.19 and 4.41‰) and $\delta^{18}O$ (mean between −3.50 and −1.63‰, Fig. 8). The monthly $\delta^{2}H$ and $\delta^{18}O$ values at both lowland and highland sites are strongly correlated when plotted separately, and characterized with LMWL of equations $\delta^{2}H = (7.57 \pm 0.13)\delta^{18}O + (15.11 \pm 0.31)$ ($R^2 = 0.96$, $p < 0.0001$) and $\delta^{2}H = (8.18 \pm 0.09)\ \delta^{18}O + (19.70 \pm 0.30)$ ($R^2 = 0.99$, $p < 0.0001$), respectively (OLSR method, Fig. 8).

The d-excess of Virunga precipitation (averaging 16.79‰ of arithmetic mean; Dataset S1) are typical of high altitude recycled continental moisture when compared to the d-excess range from the GNIP database reported in Froehlich et al., 2002 and Pfahl and Sodemann, 2014. High d-excess values are commonly a result of evaporation of both soil and surface waters at the source region under non-equilibrium conditions caused by near surface low RH coupled with strong winds (e.g. Pfahl and Sodemann, 2014). Thus, the recorded strong winds (up to 14 m s^{-1}, Fig. 5) removed the water vapor phase from the near surface before isotope equilibrium with the liquid phase was reached. Moreover, such a process induces further fractionation during moisture transportation to the condensation site. This resulted in the enrichment of $^{1}H^{2}H^{16}O$ molecules in the water vapor phase relative to $^{1}H^{1}H^{18}O$ during evaporation at source, and later in the moisture during the transportation, which led to the observed excess in the deuterium.

A d-excess difference (Δd) of 4.59‰ (calculated from d-excess values of LMWLs in Fig. 8) is observed between the low and highland sites, and increases up to ~10‰ when considering solely the d of MWLs from the least (Bweremana) and most elevated (summit) sites. Such a high Δd is indicative of the cumulative effects caused by (1) the previously mentioned kinetic fractionation during vapor formation

Table 3
Comparison of $\delta^{18}O$ and $\delta^{2}H$ of Virunga precipitation with historical (1960–1990) and modern (1991-present) datasets of precipitation from nearby central African regions, i.e. Cameroon (data are from Duala, Yaounde, Kribi, Ebolowa, Sangmélima, Somalomo, Abong-Mbang, Moloundou, and Mount Cameroon regions), Central African Republic (data are from Bangui), DR Congo (c) (data are from Kinshasa and Kinsagani), DR Congo (d) (data are from Kinshasa, Kisangani and the Virunga, this study), and Central Africa (data are from the three countries).

	$\delta^{2}H$ (‰)			$\delta^{18}O$ (‰)			d-excess (‰)			Equation of the of the Local Meteoric Water Line	Number of samples
Country	Min	Mean	Max	Min	Mean	Max	Min	Mean	Max		
Cameroon[a]	−85.50	−15.98	26.68	−10.80	−3.36	1.81	0.90	10.94	22.06	$\delta^{2}H = 7.98\delta^{18}O + 10.87$ ($R^2 = 0.96$)	208
Central African Republic[b]	−43.43	3.31	43.90	−6.83	−1.17	6.26	−11.52	12.67	20.42	$\delta^{2}H = 7.34\delta^{18}O + 11.90$ ($R^2 = 0.95$)	136
DR Congo[c]	−57.60	−14.77	26.90	−8.50	−3.56	1.03	2.90	13.83	28.40	$\delta^{2}H = 8.01\delta^{18}O + 13.86$ ($R^2 = 0.94$)	71
DR Congo[d]	−57.60	−0.05	58.89	−8.50	−2.02	6.16	−3.58	15.75	28.40	$\delta^{2}H = 7.93\delta^{18}O + 15.92$ ($R^2 = 0.96$)	294
Virunga region (this study)	−32.53	4.60	58.89	−6.44	−1.52	6.16	−3.58	16.79	23.48	$\delta^{2}H = 7.60\delta^{18}O + 16.18$ ($R^2 = 0.97$)	223
Central Africa region[e]	−85.50	−4.53	58.89	−10.80	−2.28	6.26	−11.52	13.67	28.40	$\delta^{2}H = 7.97\delta^{18}O + 13.61$ ($R^2 = 0.95$)	638

[a] Njitchoua et al., 1999; Gonfiantini et al., 2001; Wirmvem et al., 2016 and IAEA/WMO, 2017.
[b] IAEA/WMO, 2017.
[c] IAEA/WMO, 2017.
[d] IAEA/WMO, 2017, this study.
[e] Njitchoua et al., 1999; Gonfiantini et al., 2001; Wirmvem et al., 2016, IAEA/WMO, 2017 and this study.

at the source and moisture transportation, and (2) the difference of moistures affecting the low and highlands in the study area (further discussed below). A third reason, but somehow linked to the second, is the secondary processes affecting raindrops during their fall and which modify the isotopic composition of the pristine rainwater. In fact, during the fall, raindrops interact with the isotopically enriched water vapor present in the lower atmosphere. Indeed, the lower atmosphere layer was almost water vapor saturated (annual mean RH of ~80%, monthly mean range ~70–90%) which might have favored a trend towards equilibrium between the falling raindrops and the water vapor. This phenomenon was successfully demonstrated by Stewart (1975) with raindrops falling in moderate to high RH atmosphere. The process likely contributed to the enrichment of $\delta^{2}H$ and $\delta^{18}O$ of lowland sites.

The mean precipitation-weighted $\delta^{2}H$ and $\delta^{18}O$ show strong negative correlation with elevation (Fig. 9A, B), while the d-excess shows the opposite trend of a strong positive relationship with elevation (Fig. 9C). Considering all the samplings sites, the vertical $\delta^{2}H$, $\delta^{18}O$ and d-excess gradients are respectively −0.9‰/100 m elevation (Fig. 9A), −0.2‰/100 m (Fig. 9B) and 0.3‰/100 m (Fig. 9C). For a given altitude of the study area, the $\delta^{2}H$, $\delta^{18}O$ and d-excess can thus be roughly estimated by the equations $\delta^{2}H$ (‰) = (−0.007 ± 0.0009)z + (13.61 ± 2.17) (Fig. 9A), $\delta^{18}O$ (‰) = (−0.001 ± 0.0001)z + (0.29 ± 0.30) (Fig. 9C) and d (‰) = (0.003 ± 0.0002)z + (11.33 ± 0.51) (Fig. 9C), were z represents the altitude. This altitude effect is due to the earlier discussed enrichment of the falling raindrops and to the difference in moistures affecting the lowlands and highlands. Similar enrichments gaps are often observed between precipitation from low and high elevation sites of mountain valleys, and on the lee side of a mountain range. This process is commonly referred to as the pseudo-altitude effect (e.g. Moser and Stichler, 1971; Gonfiantini et al., 2001; Giustini et al., 2016) in opposition to the primary altitude effect related to the Rayleigh rainout effect (Dansgaard, 1964).

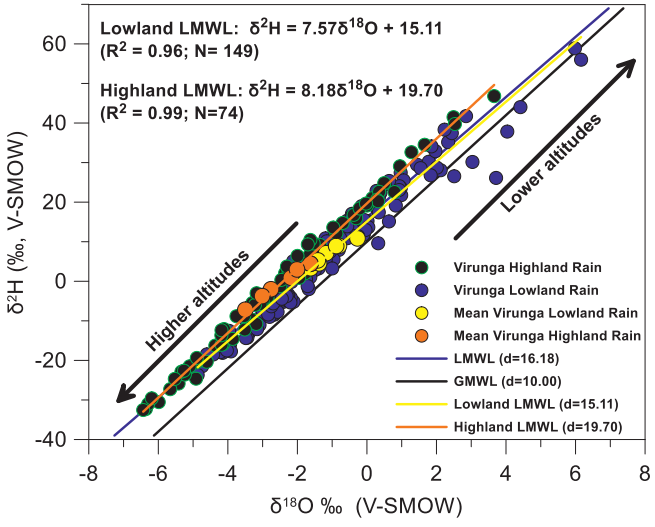

Fig. 8. Relationship between $\delta^{2}H$ and $\delta^{18}O$ from monthly, mean lowland and highland rainwater at Mt. Nyiragongo and the surrounding in the Eastern Democratic of the Congo, between December 2013 and October 2015. The lowland and highland refer to areas situated below and above 2000 m a.s.l., respectively; the whole sampling sites being between 1460 and 3470 m a.s.l of altitude.

As noted earlier, the difference in the moisture affecting highland and lowland areas is the predominant factor yielding the observed differences in $\delta^{2}H$, $\delta^{18}O$ and d-excess between the low and highland sites of the study area. In the Virunga, highland sites receive precipitation from the upper atmosphere which is produced from remote moisture sources, whereas the lowland sites are additionally affected by strictly local water vapor (Fig. 6). The altitudinal effects on $\delta^{2}H$, $\delta^{18}O$ and d-excess described by Dansgaard (1964) can thus be found by considering separately lowland and highland sites. When considered separately, the lowland sites show almost the half of the $\delta^{2}H$ and $\delta^{18}O$ gradients (−0.6‰/100 m and −0.1‰/100 m elevation, respectively) of the highland sites corresponding to −1.0‰/100 m for $\delta^{2}H$ (Fig. 9A), and −0.2‰/100 m for $\delta^{18}O$ (Fig. 9B). On the contrary, the d-excess gradient of the lowland sites (0.5‰/100 m) showed the double value of the highland sites (0.3/100 m, Fig. 9C). The difference of slopes at lowland and highland sites also contributes to their difference in gradients. The lowland area is characterized with progressive topography change (Fig. 1) yielding low slope changes (the difference of height between the lower and higher elevated sites (Δz) is only ~500 m) contrary to highland sites characterized with abrupt topography change with Δz of ~1500 m. Altogether, these differences of $\delta^{2}H$ and $\delta^{18}O$ at low and high sites cannot be linked to difference of condensation temperatures since precipitation falling at the two areas condense at similar altitudes.

4.3. Temporal variabilities of $\delta^{2}H$, $\delta^{18}O$ and d-excess

4.3.1. $\delta^{2}H$, $\delta^{18}O$ and d-excess Seasonality

Monthly $\delta^{2}H$ and $\delta^{18}O$ showed a clear seasonality which was largely consistent with local seasonal variations (Figs. 10, 11). The LMWL for the wet period (OLRS method; Fig.10A) is very similar to the equation of the LMWL from the PWLSR method of equation $\delta^{2}H = (7.52 \pm 0.12)\ \delta^{18}O + (15.50 \pm 0.38)$ ($R^2 = 0.96$). On the contrary, the effect of the precipitation amount decrease during the dry season is noticeable because the equation from the OLRS method (Fig. 10A) has both a lower slope and intercept compared to those in $\delta^{2}H = (7.05 \pm 0.19)\ \delta^{18}O + (19.77 \pm 0.34)$ ($R^2 = 0.95$) obtained with the PWLSR method. Enriched $\delta^{2}H$ and $\delta^{18}O$ were thus obtained during the dry periods,

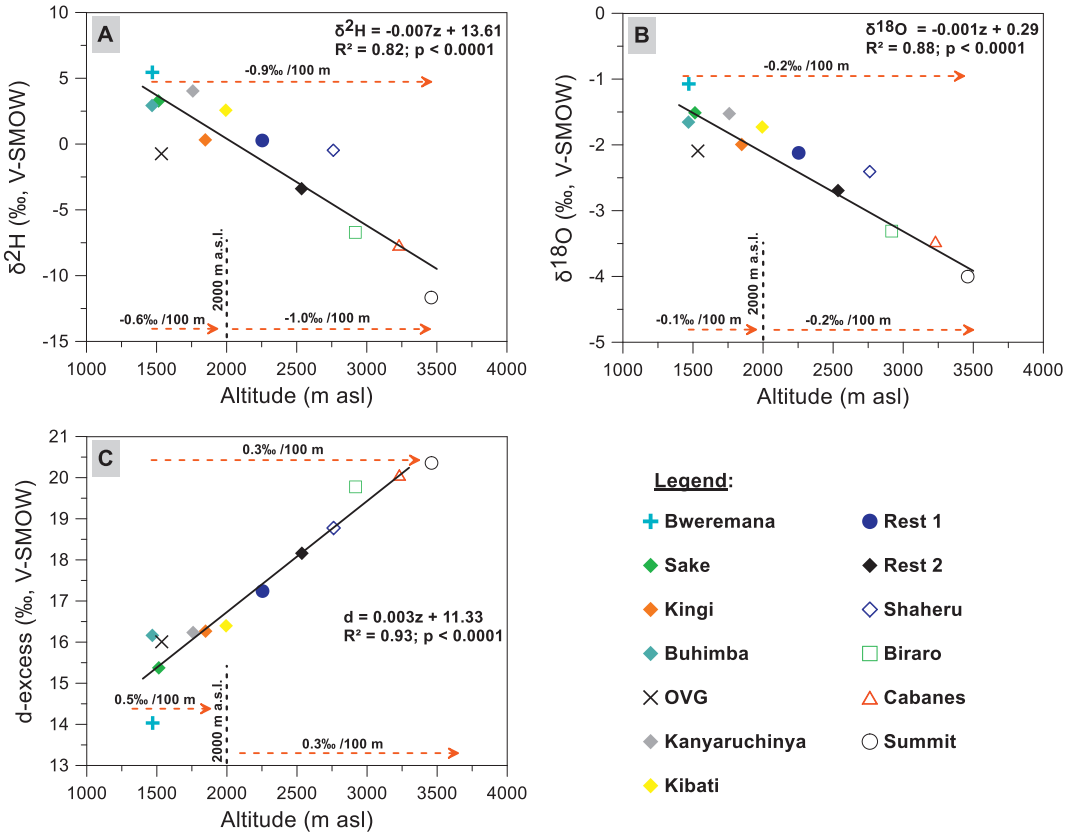

Fig. 9. Plots of mean precipitation-weighted δ^2H, $\delta^{18}O$ and d-excess versus altitude, obtained from stable isotope data from rainwater samples collected monthly at Mt. Nyiragongo and its surroundings in the Eastern Democratic of the Congo between December 2013 and October 2015. The black solid lines represent best-fit linear regression lines. The upper dotted brick-red lines show respectively the altitudinal variation of δ^2H (A), $\delta^{18}O$ (B) and d-excess (C) from the lower (i.e. Bweremana, 1460 m a.s.l.) to the highest sites (3460 m a.s.l.), whereas the lower dotted brick-red lines show the altitudinal variation of δ^2H (A), $\delta^{18}O$ (B) and d-excess (C) for the sampling sites of lowland (1470 to 2000 m a.s.l.) and highland (2000 to 3460 m a.s.l.).

while the wet periods showed depleted δ^2H and $\delta^{18}O$ values (Fig. 11). Most intermediate values were obtained during the transition periods from the wet to the dry seasons and vice versa (Fig. 10A). The large contrast between the δ^2H and $\delta^{18}O$ from dry and wet periods is more evident in Fig. 10B where mean values calculated from samples collected in dry and wet months are plotted. The dry period includes samples collected in the main dry season of July to August and those from the short dry season of January to February. Samples from the rest of the months are listed in the rainy season, and thereafter referred to as wet period group.

The higher δ^2H and $\delta^{18}O$ values that characterize the dry periods are commonly attributed to an increase in surface and soil-water evaporation during these periods. In general, the increase of evaporation is a response to temperature increase which then allows more isotopically heavy water molecules to reach the vapor phase, and later the moisture that condenses. Any given station of the Virunga region shows very weak variation of mean monthly air temperature on an annual timescale (Fig. S1 and Dataset S2). As a consequence, the observed important δ^2H and $\delta^{18}O$ seasonal behavior cannot be attributed to the recorded weak air temperature variation. This seasonality is rather the result of

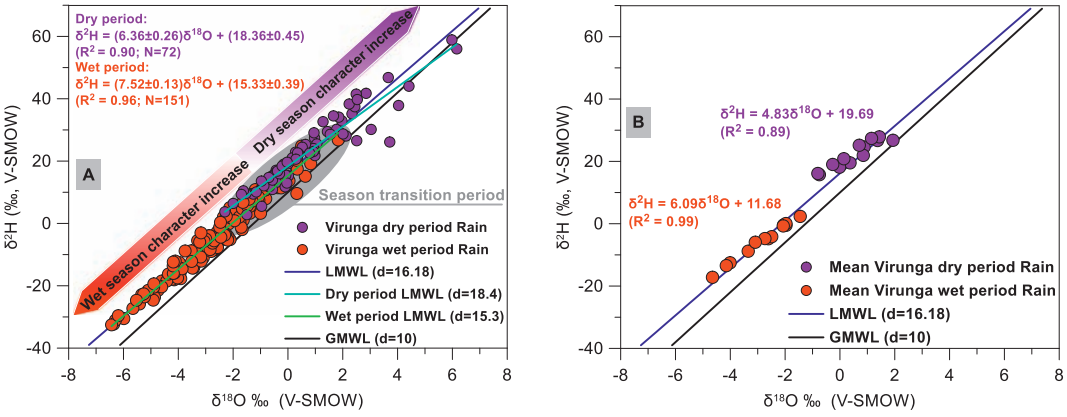

Fig. 10. Plots of monthly δ^2H versus $\delta^{18}O$ (A) and mean δ^2H versus $\delta^{18}O$ (B) in precipitations at Mount Nyiragongo and the surrounding, in the Eastern Democratic of the Congo, between December 2013 and October 2015. The red dots represent δ^2H and $\delta^{18}O$ from rainwater samples collected during the wet periods (mainly the rain season) while the violet dots represent values from dry periods (mainly dry the season).

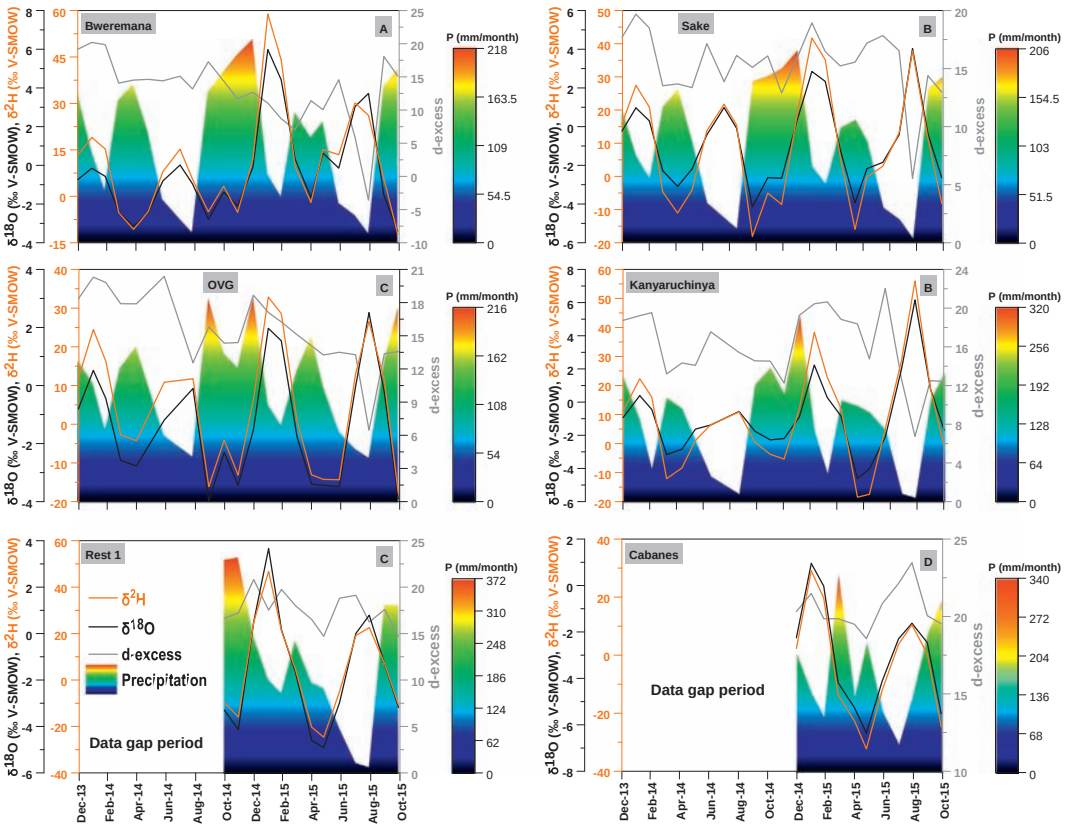

Fig. 11. Temporal evolution of monthly δ^2H, $\delta^{18}O$ and d-excess in precipitation at Mount Nyiragongo and its surroundings, in the Eastern Democratic of the Congo, between December 2013 and October 2015. The monthly precipitation values are shown in each plot to highlight the changes in monthly δ^2H, $\delta^{18}O$ and d-excess as a response to monthly precipitation change.

cumulative effects induced by the variation of interplaying meteorological parameters, including precipitation amounts, RH, air temperature and wind direction changes. The precipitation amount is negatively related to δ^2H and $\delta^{18}O$ (Fig. 11A–D) and is the key parameter driving their seasonality. In fact, while the precipitation is gradually becoming scarce during rainy to dry season transition periods, the RH similarly

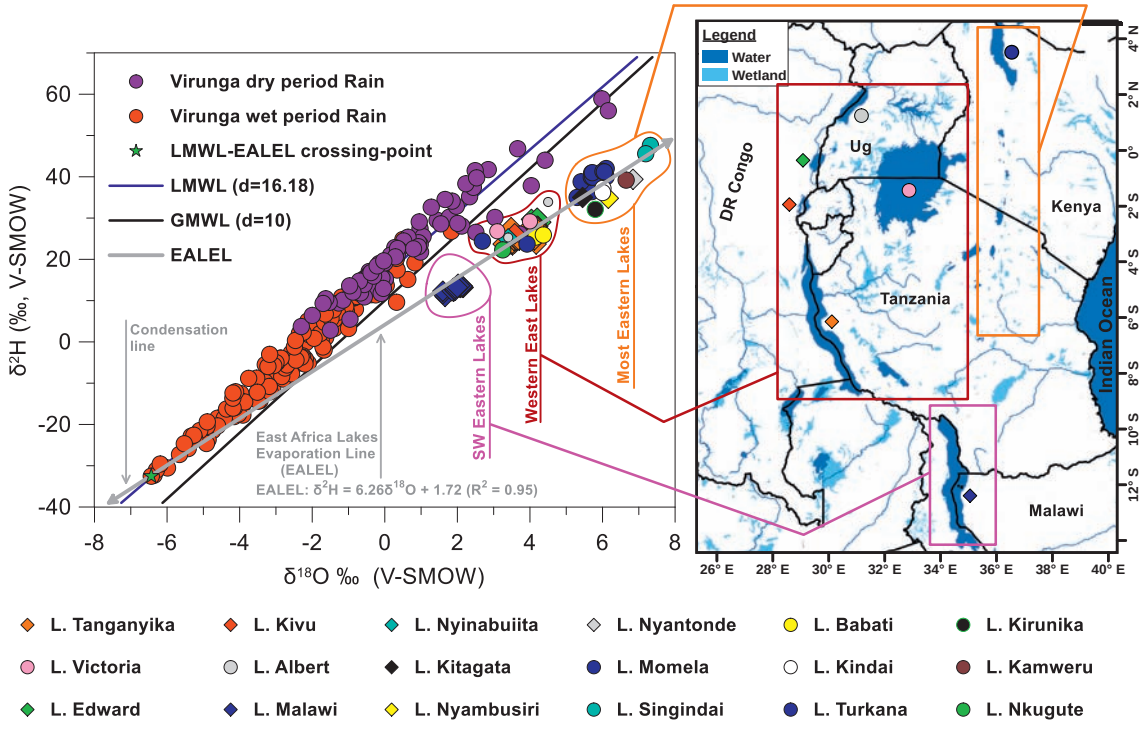

Fig. 12. Plot of oxygen and hydrogen isotope composition for Virunga precipitation and East African lakes surface waters. The lakes in the East African lakes group are located to the East of the longitude E35°, the western group are to its west, and the southwestern group is similarly found to the west with a further southward trend. Data for Virunga precipitation are from this study, lakes data are from Craig, 1975, Gonfiantini et al., 1979; Cerling et al., 1988; Odada, 2001; Bahati et al., 2005; Cockerton et al., 2013 and Jasechko et al., 2013.

Table 4
Oxygen and hydrogen stable isotopes composition of historical (1960–1990) to modern (1991-present) precipitation and rivers of the regions where moisture for the Virunga originate. The moisture source regions were deteremined using the HYSPLIT (Hybrid Single-Particle Lagrangian Integrated Trajectories) backward trajectory model developed by the Air Source Laboratory of the National Oceanic and Atmospheric Administration. The Lake Edward tributaries are both from Uganda and DR Congo territories.

Country	Station	Type	Latitude (°)	Longitude (°)	Elevation (m a.s.l.)	δ^2H (‰)			δ^{18}O (‰)			d-excess (‰)			Number of samples	References
						Min	Mean	Max	Min	Mean	Max	Min	Mean	Max		
Uganda	Entebbe	Rain	0.05	32.45	1155	−81.20	−3.61	32.04	−11.60	−2.00	4.66	−9.58	12.35	27.10	218	IAEA/WMO, 2017
	Jinja	Rain	0.45	33.20	1181	−46.73	4.02	69.18	−6.84	−0.86	11.41	−22.10	10.88	19.84	65	IAEA/WMO, 2017
	Wobulenzi	Rain	0.73	32.53	1150	−4.90	15.52	36.90	−2.50	0.09	3.30	9.40	14.81	19.70	8	IAEA/WMO, 2017
	Rukungiri	Rain	−0.84	29.94	1595	−37.70	0.37	44.20	−6.14	−1.69	4.66	3.68	13.93	23.72	26	IAEA/WMO, 2017
	Soroti	Rain	1.69	33.62	1038	−59.10	−9.97	19.67	−8.89	−2.81	0.51	9.14	12.49	15.59	14	IAEA/WMO, 2017
	Kisoro	Rain	−1.28	29.69	1924	−26.00	5.70	37.60	−5.19	−0.80	4.10	4.38	12.09	20.28	8	IAEA/WMO, 2017
	Masaka	Rain	−0.33	31.76	1306	−35.73	−5.56	21.60	−5.90	−2.17	2.05	4.40	11.83	15.66	45	IAEA/WMO, 2017
	Bukasa Island	Rain	−0.41	32.53	1240	−16.80	15.00	41.40	−3.44	0.83	4.42	−1.98	8.35	17.38	24	IAEA/WMO, 2017
	Bugondo	Rain	1.69	33.62	1038	−22.90	1.60	22.50	−4.55	−1.52	0.93	8.18	13.80	18.96	39	IAEA/WMO, 2017
	Lake Edward major tributaries	River				−18.40	−2.80	10.60	−4.70	−2.15	0.20	7.90	14.42	19.80	25	Russell and Johnson, 2006 Cockerton et al., 2013
Rwanda	Rwasave	Rain				−34.10	−10.52	13.75	−6.63	−3.55	−0.38	14.93	17.91	22.88	11	Munyaneza et al., 2012
	Murama	Rain				−42.19	−8.41	13.71	−7.15	−3.23	−0.34	13.88	17.39	20.40	11	Munyaneza et al., 2012
	Mubumbano	Rain				−42.50	−11.09	19.19	−7.59	−3.59	−0.23	11.40	17.64	23.71	11	Munyaneza et al., 2012
	Kibilizi	Rain				−55.20	−14.18	5.82	−8.90	−4.01	−1.08	14.48	17.90	22.23	10	Munyaneza et al., 2012
	Gisunzu	Rain				−33.64	−6.34	18.27	−6.48	−2.88	0.35	10.36	16.73	19.17	11	Munyaneza et al., 2012
	Rwabuye	River				−2.11	−1.33	−0.56	−1.24	−1.17	−1.11	7.82	8.05	8.29	2	Munyaneza et al., 2012
	Migina	River				−9.82	−8.78	−7.73	−2.47	−2.43	−2.38	9.97	10.64	11.31	2	Munyaneza et al., 2012
	Akagera	River				−16.53	−13.34	−10.15	−3.42	−3.41	−3.40	10.84	13.94	17.04	2	Munyaneza et al., 2012
	Mukura	River				−13.14	−9.75	−2.92	−3.49	−2.85	−1.73	10.91	13.05	16.17	6	Munyaneza et al., 2012
	Kansi	River				−25.68	−12.37	−2.35	−4.96	−3.11	−1.15	5.29	12.36	17.84	78	Munyaneza et al., 2012
Kenya	Kericho	Rain	−0.37	35.35	2130	−53.10	−10.04	23.00	−7.90	−2.89	0.81	−8.84	13.10	23.10	19	IAEA/WMO, 2017
	Muguga	Rain	−1.22	36.63	2070	−35.10	−12.07	16.40	−6.18	−3.33	−0.42	6.30	14.60	22.48	14	IAEA/WMO, 2017
	Multiple	Rain	from −1.90 to 3.95	from 35.12 to 37.53	from 362 to 2019	−37.00	−4.09	17.40	−5.90	−2.48	1.90	1.80	15.76	40.90	16	Levin et al., 2009
	Multiple	Rain	from −3.42 to 3.72	from 35.33 to 38.70	from 300 to 3078	−48.00	−12.46	36.00	−7.00	−3.04	6.60	−16.80	11.88	32.40	66	Levin et al., 2009
Tanzania	Dodoma	Rain	−6.03	35.66	1120	−33.80	−11.03	11.70	−5.88	−3.14	0.06	11.22	14.11	17.88	3	IAEA/WMO, 2017
	Arucha	Rain				−1.60	−1.60	−1.60	−1.20	−1.20	−1.20	8.00	8.00	8.00	1	Mduma et al., 2016
	Arucha	Spring				−15.00	−11.20	−3.90	−2.50	−2.07	−1.30	2.00	5.36	9.70	10	Mduma et al., 2016

decreases and thence even a small increase of air temperature leads to significant increase in surface water evaporation. Similarly the soil-plants evapotranspiration will progressively decrease with dry season approaching (Fig. 3), because soil-water content decreases (Fig. 4). It should be noted that transpired water vapor by plants tends to be isotopically similar to the liquid water drawn into its roots (e.g. Harwood et al., 1998 and Wang et al., 2012). The residual soil-water and the open surface water that are then evaporating will be gradually formed of heavier isotopes water vapor. A reverse process will be observed during transition periods from dry to wet season.

The moisture source regions for the study area abound in perennial, small to large open surface waters (Figs. 2B, 3 and 4), particularly lakes of isotopically enriched surface waters (see discussion in Section 4.3.2.), which represents the predominant source of vapor for the atmosphere during the dry periods. On the other hand, a peak is observed in the soil-water saturation during the rainy months (Fig. 4), periods during which the proportion of water vapor from soil-plants evapotranspiration in the atmosphere predominates. The vapor from rainy season is isotopically depleted because it is from freshly precipitated rains and due to the high precipitation amount recorded in this period. Therefore, the resulting precipitation will show depleted δ^2H and $\delta^{18}O$ values in the rainy periods and enriched in the dry (Fig. 11A–D). The season transition periods start from mid-January and late June for the transition from wet to dry periods, and from late February and early or mid-September for the transition from dry to wet season. However, the duration of this transition period varies from year to year, and is becoming longer as consequence of the ongoing climate change. The season transition periods were particularly marked with intermediate δ^2H and $\delta^{18}O$ values between the most enriched in the dry and the most depleted in the wet periods (Fig. 10A).

4.3.2. Stable isotope variability in relation to moisture source dynamics and weather patterns

The changes of wind direction (Fig. 5) bring moisture from different sources to the study area (Fig. 6), which might yield variation in the isotopic composition of precipitation. On a more extended regional scale, the equatorial East African region experiences three major air streams: the northeast monsoon system, the southeast monsoon system from the Indian Ocean and the southwesterly humid air from the Congo basin (Nicholson, 1996). The shifting between the northeast and southeast monsoons and their strength controls the seasonal distribution of precipitation in East Africa (Levin et al., 2009). The monsoon systems are in turn controlled by the Indian Ocean surface temperature change (Tierney et al., 2013). The influence from the Indian Ocean on precipitation variability is limited to the Kenyan and Tanzanian coastal and continental lands (Ummenhofer et al., 2009; Lyon and DeWitt, 2012; Tierney et al., 2013). This limitation is caused by the Ethiopian, Kenyan and Somalia plateau and mountains that block the northeast and southeast airstreams from penetrating further west in the continent (Slingo et al., 2005; Levin et al., 2009). Moreover, the Virunga mountain belt (Fig. 1) forms a wind barrier that maintains the dominant and strong NE, E and SE originating winds in the upper atmosphere (Fig. S3), while the calmer winds from the S and SW are maintained in the lower atmosphere (Fig. S2). These NE, E and SE winds are accordingly charged with moisture evaporated from the Lake Edward and Lake Albert surface waters (Fig. 6), and that evapotranspired in their moderately to densely forested catchments (Fig. 2B) and beyond. The moisture from evapotranspiration in Lake Victoria and its southwestern catchment reach the study area through the E and SE winds. On the contrary, the S and SW winds of the lower atmosphere carry moisture evapotranspired in the Tanganyika-Kivu basins especially that evaporated from the neighboring Lake Kivu. Furthermore, the NE and E originating high-speed air mass moves upward as a result of topography change and might thus yield orographic lifting at Virunga Mountains. Hence, the NE and *E*-SE originating moistures mainly influence the δ^2H and $\delta^{18}O$ of precipitation of highland sites, whereas the S and SW low-level moistures additionally influence that of lowland sites. The high speed of the NE and E-SE winds yields the earlier discussed kinetic fractionation which leads to the higher d-excess values that characterize the precipitation of highland sites. On the contrary, the S-SW winds in the lower atmosphere are less strong (Fig. 5) and favor a relatively equilibrium fractionation in conjunction with the high RH prevailing in lowland areas. Because of the topographic constraints and the lack of unidirectional strong winds, this S to SW originating moisture is almost permanent in the lower atmosphere as revealed by the backward trajectory plots (Fig. 6), and drives the earlier noted isotopic enrichment of the falling rain drops.

The change in the moisture source region is not the only way in which the moisture isotopic composition varies, and yield variation in δ^2H and $\delta^{18}O$ of precipitation. Indeed, it is essential to consider the fact that the atmospheric moisture results from the mixture of water vapors from two reservoirs: the open surface waters (mainly the lakes) as the first and constant reservoir and the water stocked in soil and plants as the second. Therefore, the δ^2H and $\delta^{18}O$ of precipitation is both influenced by the moisture source region, and by the ratio of water vapor from surface water evaporation to that from soil-plants evapotranspiration. Such a dual conception of the moisture source dynamics perfectly explains the observed difference in the δ^2H and $\delta^{18}O$ of precipitation collected from two periods with similar moisture source region. For instance, from December to March the moisture originates from the NE (Fig. 6A–B) which means that precipitation from December, January, February and March would theoretically have very comparable values of δ^2H and $\delta^{18}O$. What is observed is that December and March on one side, and January and February on the other, have similar values of δ^2H and $\delta^{18}O$ respectively (Fig. 11). Certainly the amount effect and the slight evaporative enrichment of January–February could be pointed out as the causes for the observed variation. Nevertheless, when the hydrography of the region is considered, it appears that the difference is related to a hidden parameter related to the shift in the ratio (as percentage into the atmosphere) of water vapor from each of the two reservoirs.

The surface waters of the East African lakes are strongly enriched in δ^2H and $\delta^{18}O$ (Fig. 12) because of the intense evaporation which exceeds in some cases the precipitation they receive over their surfaces (see Section 2.1). On the contrary, the precipitation, rivers and springs are depleted (Table 4) compared to surface waters from lakes of corresponding regions of East Africa. It is thus expected to have in the atmosphere a mixture of comparatively enriched water vapor from lakes evaporation and depleted water vapor from soil-plants evapotranspiration. The abundance of each is thus very decisive for the determination of δ^2H and $\delta^{18}O$ of the resulting precipitation. In the atmosphere, the water vapor from soil-plant evapotranspiration is predominant during the rainy season (because the surface undergoing evapotranspiration is larger compared to that of lakes) yielding isotopically depleted precipitation, contrary to the dry season when water vapor from the lakes predominates yielding isotopically enriched precipitation.

The δ^2H, $\delta^{18}O$ and d-excess of Virunga precipitation (Table 1) are thus intermediate between those of precipitation in the moisture source regions (Table 4) and that of surface waters of East African lakes (Fig. 12). These lakes are subdivided into the most eastern, western and southwestern groups (Fig. 12) based on the δ^2H and $\delta^{18}O$ values of their surface waters. The western lakes of East Africa (e.g. Lake Tanganyika, Victoria, Albert, Edward, or Kivu) have surface waters with intermediate δ^2H and $\delta^{18}O$ values between the highly enriched most eastern lakes of semi-arid and savanna regions (e.g. Lake Turkana in Kenya and Lake Singidai in Tanzania) and less enriched southwestern lakes (e.g. Lake Malawi, Fig. 12). Virunga wet season samples show lower d-excess (Fig. 10) consistent with the higher RH recorded this period (Fig. S1). In the dry season in contrast, after the season transition period (Fig. 10), the δ^2H and $\delta^{18}O$ of precipitation deviate from their regular alignment along the LMWL

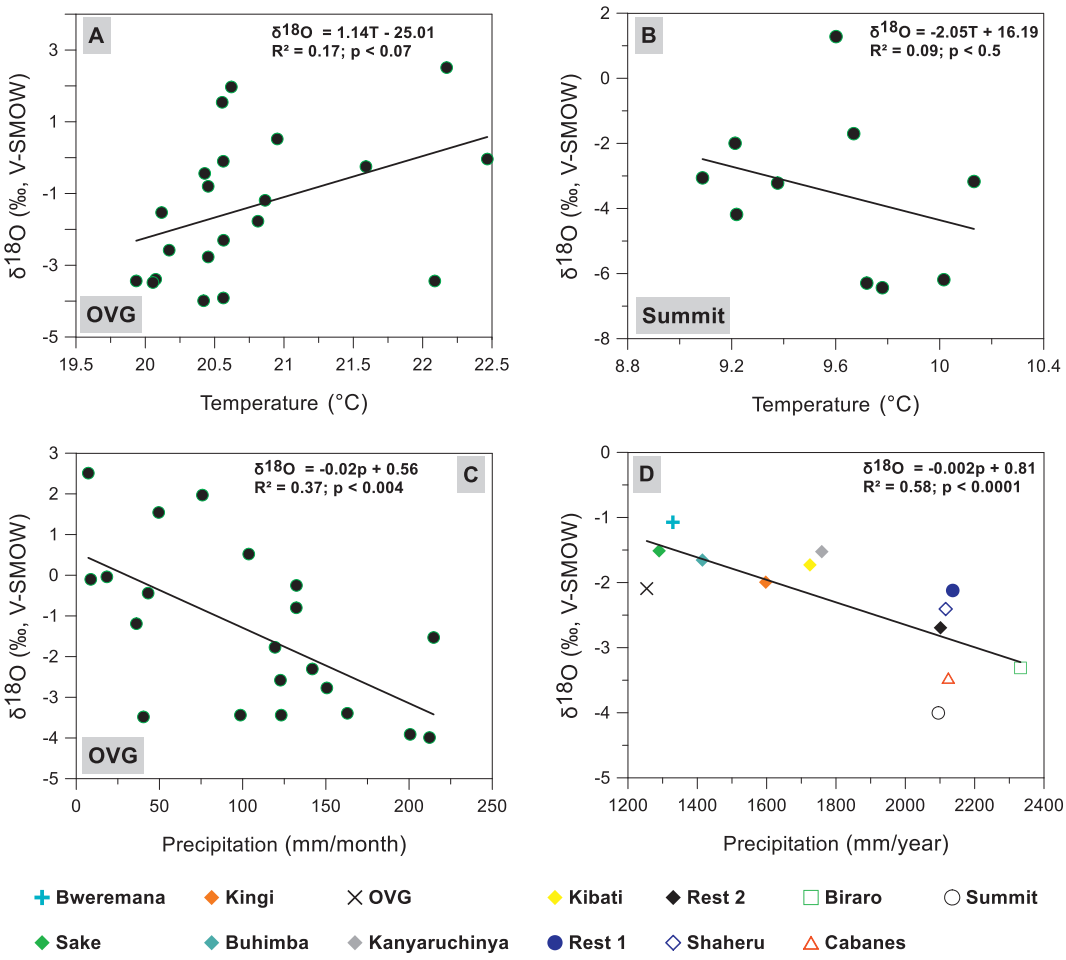

Fig. 13. Relationship between monthly $\delta^{18}O$ and monthly mean temperature at OVG (A) and the Nyiragongo summit (B), precipitation-weighted $\delta^{18}O$ and mean monthly precipitation at OVG (C), and whole sites precipitation-weighted $\delta^{18}O$ and their mean annual precipitation (D). Oxygen stable isotope data are from precipitation collected monthly at Mt. Nyiragongo and the surroundings, in the Eastern Democratic of the Congo, between December 2013 and October 2015. The legend refers only to D.

and show an arid-like evaporative trend (Fig. 12). The latter reflects the increased fingerprint of water vapor from lakes evaporation, and results in precipitation with δ^2H and $\delta^{18}O$ close to that of the west and most eastern East African lakes. Some precipitation from the dry periods even plots in the same area as the western East African lakes such as Tanganyika, Victoria, Edward, Kivu and Albert (Fig. 12). The linear regression line for East African Lakes representing the East African Lakes Evaporation Line (EALEL: $\delta^2H = 6.26\ \delta^{18}O + 1.72$ with $R^2 = 0.95$; Fig. 12) meets the Virunga LMWL exactly at the most depleted value of Virunga precipitation. This intersection represents both the hypothetical unevaporated surface lake waters and the isotope composition of pristine precipitation which did not undergo the enrichment during the rain fall as discussed earlier. From an annual perspective, the moisture source region induces only a slight variation in the isotope composition of precipitation. This is supported by the fact that both precipitation (which later form soil-plant water) and lake surface waters from the moisture source regions have comparable δ^2H and $\delta^{18}O$ values (Fig. 12 and Table 4). They are further located in a climatically similar region, and almost originate from similar distances from the source point and might thus be equally fractioned when crossing the continent (continent effects) during moisture transportation to the condensation site. Hence, the seasonal variation of the moisture source, i.e. the shift in the ratio of water vapor from each reservoir, seems to be the primary influence on variability of precipitation δ^2H and $\delta^{18}O$, and secondly the spatial variation of moisture sources.

4.4. Oxygen isotopes — temperature and precipitation amounts relationships

The Central-Eastern Africa region air temperature shows small variation on an annual scale (e.g. Fig. S1) because of their location in the tropical zone near the equator (Fig. 1). As a consequence, the air temperature of the moisture source regions essentially coincides with that of precipitation in the study area, which results in a lack of dependency between $\delta^{18}O$ and the air temperature (Fig. 13A and B). This trend is commonly noticed in tropical regions (e.g. Rozanski et al., 1993; Bowen, 2008), and is even conserved when tropical rains are plotted along with other GNIP regions (Gat et al., 2001). The Fig. 11 roughly shows a negative relationship between precipitation amounts and $\delta^{18}O$ and δ^2H, a tendency further highlighted in Fig. 13C and D for $\delta^{18}O$.

For any given site, the monthly $\delta^{18}O$ shows a weak positive relationship with corresponding precipitation (e.g. Fig. 13C), with R^2 ranging from 0.11 (at Shaheru) to 0.37 (at OVG). Thus, the $\delta^{18}O$ dependency on precipitation amounts for the Virunga averages 2.96‰/100 mm of monthly precipitation, and varies between 2.10 and 4.51‰/100 mm. In general, the $\delta^{18}O$ precipitation amounts dependency in the study area decreases with increasing altitude (Fig. 13D). Hence, the $\delta^{18}O$ of sites closer to Lake Kivu shoreline, i.e. Buhimba, Bweremana and Sake (Fig. 1) are the most affected by precipitation amount variation, and show amount dependency of 3.30, 4.05 and 4.51‰/100 mm, respectively. This might be caused by the fact that they are the most impacted

by the heavier water vapor from the neighboring Lake Kivu, a vapor constantly present in the lower atmosphere.

5. Conclusions

This study investigated the stable isotope composition of precipitation at Mount Nyiragongo and the surrounding Virunga region, Eastern Democratic Republic of Congo, a region located on the limit between Central and Eastern Africa. We also evaluated the role of moisture source region and temporal variations, and of weather patterns on Virunga precipitation $\delta^{18}O$ and $\delta^{2}H$ spatial distribution and seasonality. These are the first results of $\delta^{18}O$ and $\delta^{2}H$ of precipitation to be reported for this region. They thus broaden the GNIP network and reduce gaps and uncertainties in the global estimation of $\delta^{18}O$ and $\delta^{2}H$ temporal and spatial variations in precipitation. The reduction of gaps and uncertainties will yield the improvement of environmental and climatic modelling using data reported in this study.

Our results imply that Virunga precipitation originate from high altitude recycled continental moisture, and we defined the first Local Meteoric Water Line (LMWL) for this region. The slope of the LMWL reveals that during condensation, rainwater forms under equilibrium conditions, which is common in central Africa forest regions and makes the Virunga part of this region. On the other hand, both the LMWL higher intercept and $\delta^{18}O$ values differentiate this region from Central African forest regions, and make the Virunga closer to the East Africa region. Such a dual membership is both in line with Virunga region position between central and Eastern Africa, and the convergence zone-like around the study area where the N-NE and S-SW trade winds come together.

A topographically induced $\delta^{2}H$, $\delta^{18}O$ and d-excess spatial variation is observed in the study area, and divides the sampling sites into two groups: the lowland sites characterized by higher $\delta^{2}H$ and $\delta^{18}O$ and lower d-excess values, and the highland sampling sites with lower $\delta^{2}H$ and $\delta^{18}O$ and higher d-excess values. The two groups are further observed based on weather patterns such as the temperature (temperature is lower at highland and higher at lowland areas), wind speed and directions (high speed and of well-defined direction at highland, calm and generally lacking of unique-direction at lowland) or precipitation (higher and lower precipitation at highland and lowland areas, respectively). For wind direction and speed, they yield two moisture source regions in the upper and lower atmosphere, respectively. The NE-E originating high speed winds of the upper atmosphere brought moisture from the Nile River basin yielded depleted precipitation at the highlands. On the other hand, the S-SW warding calm winds of the lower atmosphere carried the moisture from the Congo River basin. The southern wind is principally charged with enriched moisture evaporated from the neighboring Lake Kivu, which favored the isotope enrichment of lowland precipitation.

The monthly $\delta^{2}H$ and $\delta^{18}O$ showed a well-defined seasonality linked to local season variation. The heavier $\delta^{2}H$ and $\delta^{18}O$ were therefore obtained during the dry periods and the lighter, in the wet periods, and were particularly correlated to precipitation amount. In the Virunga region two reservoirs are sources for atmospheric water vapor: the isotopically enriched permanent surface water of the East African Great Lakes and the depleted water vapor from soil-water and plants. During the dry period vapor from lakes evaporation dominates in the atmosphere yielding isotopically enriched precipitation, while in the rainy season vapor from soil-plants evapotranspiration is dominant producing depleted precipitation. Thus, the seasonality of Virunga precipitation isotope composition was driven by the cumulative effects of the changes in evaporation rate as a consequence of slight variation of air temperature and Relative Humidity, the precipitation amount variation, and the seasonal and spatial variation in the moisture sources.

Finally, no $\delta^{18}O$ dependency on air temperature was observed, as is generally the case for tropical regions since the air temperature of the moisture source region essentially coincides with that in the precipitation area. However, a negative relationship between precipitation amounts and $\delta^{18}O$ and $\delta^{2}H$ was observed, their dependencies decrease with increasing altitude. Thus, sites located on the shoreline of Lake Kivu showed a higher dependency on precipitation amounts, because they are the most impacted by the heavier water vapor from this lake, a vapor which is permanent in the lower atmosphere and that mediates the isotope enrichment of falling raindrops.

Supplementary dataset related to this paper can be found in the enclosed Dataset 1 and Dataset 2 (XLS files). Supplementary data to this article can be found online at https://doi.org/10.1016/j.scitotenv.2018.01.284.

Author contributions

Charles M. Balagizi conceived the study and the samples collection protocol, the latter was then commented by Marcello Liotta, Emilio Cuoco and Marcellin M. Kasereka. The field works were carried out by Charles M. Balagizi and Marcellin M. Kasereka. Charles M. Balagizi analyzed the data and drafted the manuscript which were latter considerably commented, amended and then approved by all the co-authors.

Acknowledgments

Part of the water samples were analyzed by the International Atomic Energy Agency (IAEA, Isotope Hydrology Laboratory) within the framework of the Global Network of Isotopes in Precipitation. Ygor Oliveri and Aldo Sollami of INGV-Palermo carried out additional analyses. Stefan Terzer-Wassmuth (IAEA, Vienna) and Wendy McCausland (U.S. Geological Survey) provided insightful comments on an earlier version of the manuscript, and Dr. Omar Munyaneza of the National University of Rwanda kindly shared published Rwandan precipitation and river stable isotopes data. The authors thank the rangers of the Virunga National Park for security assistance during field activities, and all the inhabitants that accepted the installation of the rain-gauges in their fields. Horizontal wind component and air temperature data at Nyiragongo summit were obtained from the ECMWF (European Centre for Medium-Range Weather Forecasts) MARS archive under license from the Italian Air Force Meteorological Service. We also acknowledge useful comments and recommendations from Polona Vreca and two others anonymous reviewers, which improved the manuscript, and the editorial handling of Ralf Ludwig.

References

Aggarwal, P.K., Romatschke, U., Araguas-Araguas, L., Belachew, D., Longstaffe, F.J., Berg, P., Schumacher, C., Funk, A., 2016. Proportions of convective and stratiform precipitation revealed in water isotope ratios. Nat. Geosci. 9 (8):624–629. https://doi.org/10.1038/ngeo2739.

Akkermans, T., Thiery, W., van Lipzig, N., 2014. The regional climate impact of a realistic future deforestation scenario in the Congo Basin. J. Clim. 27, 2714–2734 (doi: JCLI-D-13-00361.1).

Allen, R.G., Pereira, L.S., Raes, D., Smith, M., 1998. Crop Evapotranspiration: Guidelines for Computing Crop Requirements. Irrigation and Drainage Paper No. 56. FAO, Rome, Italy.

Bahati, G., Pang, Z., Armannsson, H., Isabirye, E.M., Kato, V., 2005. Hydrology and reservoir characteristics of three geothermal systems in Western Uganda. Geothermics 34, 568–591.

Balagizi, M.C., Darchambeau, F., Yalire, M.M., Bouillon, S., Borges, V.A., 2015. River geochemistry, chemical weathering, and atmospheric CO_2 consumption rates in the Virunga Volcanic Province (East Africa). Geochem. Geophys. Geosyst. 16:2637–2660. https://doi.org/10.1002/2015GC005999.

Balagizi, M.C., Yalire, M.M., Ciraba, M.H., Vicky, B.K., Minani, S.A., Kinja, K.A., Kasereka, M. M., 2016a. CO_2 and SO_2 emissions, temperature variations and field observations before and after the February 29, 2016 new vent inside Nyiragongo crater. Bull. Volcanol. 78:64. https://doi.org/10.1007/s00445-016-1055-y.

Balagizi, M.C., Kasereka, M.M., Terzer, S., Cuoco, E., Liotta, M., 2016b. Identifying hydrological pathways in the north basin of Lake Kivu using stable isotope ratios of meteoric recharge and surface water. Geophysical Research Abstracts Vol. 18, EGU2016-9720-1, EGU General Assembly, Vienna.

Balagizi, M.C., Kasereka, M.M., Cuoco, E., Liotta, M., 2017. Rain-plume interactions at Nyiragongo and Nyamulagira volcanoes and associated rainwater hazards, East Africa. Appl. Geochem. 81, 76–89.

Barasa, B., Kakembo, V., Mugaga, F., Egeru, A., 2013. Comparison of extreme weather events and streamflow from drought indices and a hydrological model in River Malaba, Eastern Uganda. Int. J. Environ. Stud. 70 (6), 940–951.

Bobrowski, N., Giuffrida, G.B., Yalire, M., Lübcke, P., Arellano, S., Balagizi, C., Calabrese, S., Galle, B., Tedesco, D., 2016. Multi-component gas emission measurements of the active lava lake of Nyiragongo, DR Congo. J. Afr. Earth Sci.:1–10 https://doi.org/10.1016/j.jafrearsci.2016.07.010.

Boke-Olén, N., Abdi, A., Hall, O., Lehsten, V., 2017. High-resolution African population projections from radiative forcing and socio-economic models, 2000 to 2100. Sci. Data 4: 160130. https://doi.org/10.1038/sdata.2016.130.

Bowen, G., 2008. Spatial analysis of the intra-annual variation of precipitation isotope ratios and its climatological corollaries. J. Geophys. Res. 113 (D05113). https://doi.org/10.1029/2007JD009295.

Brawn, J.D., Benson, T.J., Stager, M., Sly, N.D., Tarwater, C.E., 2017. Impacts of changing rainfall regime on the demography of tropical birds. Nat. Clim. Chang. 7:133–136. https://doi.org/10.1038/nclimate3183.

Bultot, F., 1993. Evaporation from a tropical lake: comparison of theory with direct measurements. Comment. J. Hydrol. 143, 513–519.

Bussmann, R.W., 2006. Vegetation zonation and nomenclature of African Mountains - an overview. Lyonia 11, 41–66.

Cerling, T.E., Bowman, J.R., O'Neil, J.R., 1988. An isotopic study of a fluvial lacustrine sequence: the Plio-Pleistocene Koobi Fora sequence, East Africa. Palaeogeogr. Palaeoclimatol. Palaeoecol. 63, 335–356.

Chadwick, R., Good, P., Martin, G., Rowell, D.P., 2016. Large rainfall changes consistently projected over substantial areas of tropical land. Nat. Clim. Chang. 6 177-18. https://doi.org/10.1038/nclimate2805.

Christy, J.R., Norris, W.B., McNider, R.T., 2008. Surface temperature variations in East Africa and possible causes. J. Clim. 22, 3342–3356.

Cockerton, H.E., Street-Perrott, F.A., Leng, M.J., Barker, P.A., Horstwood, M.S.A., Pashley, V., 2013. Stable-isotope (H, O, and Si) evidence for seasonal variations in hydrology and Si cycling from modern waters in the Nile Basin: implications for interpreting the quaternary record. Quat. Sci. Rev. 66:4–21. https://doi.org/10.1016/j.quascirev.2012.12.005.

Coplen, T.B., Wildman, J.D., Chen, J., 1991. Improvements in the gaseous hydrogen-water equilibration technique for hydrogen isotope-ratio analysis. Anal. Chem. 63, 910–912.

Coppola, D., Campion, R., Laiolo, M., Cuoco, E., Balagizi, M.C., Ripepe, M., Cigolini, C., Tedesco, D., 2016. Birth of a lava lake: Nyamulagira volcano 2012–2015. Bull. Volcanol. 78:20. https://doi.org/10.1007/s00445-016-1014-7.

Craig, H., 1961. Isotopic variations in meteoric waters. Science 133, 1702–1703.

Craig, H., 1975. Lake Tanganyika Geochemical and Hydrographic Study: 1973 Expedition. Scripps Institute of Oceanography La Jolla, California (Report 75–5, 83 p).

D'Alessandro, W., Federico, C., Longo, M., Parello, F., 2004. Oxygen isotope composition of natural waters in the Mt. Etna area. J. Hydrol. 296, 282–299.

Dansgaard, W., 1964. Stable isotopes in precipitation. Tellus 16:438–468. https://doi.org/10.1111/j.2153-3490.1964.tb00181.x.

Dee, D.P., Uppala, S.M., Simmons, A.J., Berrisford, P., Poli, P., Kobayashi, S., Andrae, U., Balmaseda, M.A., Balsamo, G., Bauer, P., Bechtold, P., Beljaars, A.C.M., van de Berg, L., Bidlot, J., Bormann, N., Delsol, C., Dragani, R., Fuentes, M., Geer, A.J., Haimberger, L., Healy, S.B., Hersbach, H., Hólm, E.V., Isaksen, L., Kallberg, P., Köhler, M., Matricardi, M., McNally, A.P., Monge-Sanz, B.M., Morcrette, J.-J., Park, B.-K., Peubey, C., de Rosnay, P., Tavolato, C., Thépaut, J.-N., Vitart, F., 2011. The ERA-interim reanalysis: configuration and performance of the data assimilation system. Q. J. R. Meteorol. Soc. 137:553–597. https://doi.org/10.1002/qj.828.

DeFries, R.S., Rudel, T., Uriarte, M., Hansen, M., 2010. Deforestation driven by urban population growth and agricultural trade in the twenty-first century. Nat. Geosci. 3: 178–181. https://doi.org/10.1038/ngeo756.

Diaz, H.F., Bradley, R.S., 1997. Temperature variations during the last century at high elevation sites. Clim. Chang. 36, 253–279.

Duane, W.J., Pepin, N.C., Losleben, M.L., Hardy, D.R., 2008. General characteristics of temperature and humidity variability on Kilimanjaro, Tanzania. Arct. Antarct. Alp. Res. 40 (2), 323–334.

Egeru, A., Osaliya, R., MacOpiyo, L., Mburu, J., Wasonga, O., Barasa, B., Aleper, D., Majaliwa, M.G.-J., 2014. Assessing the spatio-temporal climate variability in semi-arid Karamoja sub-region in north-eastern Uganda. Int. J. Environ. Stud. 71 (4) (490-50).

Epstein, S., Mayeda, T., 1953. Variation of O^{18} content of waters from natural sources. Geochim. Cosmochim. Acta (5), 213–224.

Eriksen, S., 2001. Linkage between climate change and desertification in East Africa part 2: policy linkages between climate change and desertification. Arid Lands 49 (May/June 2001).

FAO, 2016. Climate Change and Food Security: riSks and Responses (ISBN 978-92-5-108998-9).

Farr, T.G., Rosen, P.A., Caro, E., Crippen, R., Duren, R., Hensley, S., Kobrick, M., Paller, M., Rodriguez, E., Roth, L., Seal, D., Shaffer, S., Shimada, J., Umland, J., Werner, M., Oskin, M., Burbank, D., Alsdorf, D., 2007. The shuttle radar topography mission. Rev. Geophys. 45, RG2004. https://doi.org/10.1029/2005RG000183.

Feng, X., Porporato, A., Rodriguez-Iturbe, I., 2013. Changes in rainfall seasonality in the tropics. Nat. Clim. Chang. 3:811–815. https://doi.org/10.1038/nclimate1907.

Fontes, J.C., Olivry, J.C., 1976. Gradient isotopique entre 0 et 4000 m dans les précipitations du Mont Cameroun. C.R. Reun. Annu. Sci. Terre. Soc. Geol., Paris.

Froehlich, K., Gibson, J.J., Aggarwal, P.K., 2002. Deuterium excess in precipitation and its climatological significance. Study of Environmental Change Using Isotope Techniques. International Atomic Energy Agency, Vienna, pp. 54–65.

Gat, J.R., 2010. Isotope Hydrology: A Study of the Water Cycle. Imperial College Press, London.

Gat, J.R., Carmi, I., 1970. Evolution of the isotopic composition of atmospheric waters in the Mediterranean Sea area. J. Geophys. Res. 75, 3039–3048.

Gat, J.R., Tzur, Y., 1967. Modification of the isotopic composition of rainwater by processes which occur before groundwater recharge. Isot. Hydrol. 49–60.

Gat, J.R., Mook, W.G., Meijer, H.A., 2001. Environmental isotopes in the hydrological cycle, principles and applications. Vol. 2: Atmospheric Water, UNESCO/IAEA Series.

Gat, J.R., Klein, B., Kushnir, Y., Roether, W., Wernli, H., Yam, R., Shemesh, A., 2003. Isotope composition of air moisture over the Mediterranean Sea: an index of the air–sea interaction pattern. Tellus 55B, 953–965.

Giustini, F., Brilli, M., Patera, A., 2016. Mapping oxygen stable isotopes of precipitation in Italy. J. Hydrol. Reg. Stud. 8, 162–181.

Gonfiantini, R., Zuppi, G.M., Eccles, D.H., Ferro, W., 1979. Isotope Investigation of Lake Malawi. Proc. Int. Symp. International Atomic Energy Agency, Vienna.

Gonfiantini, R., Roche, M.A., Olivry, J.C., Fontes, J.C., Zuppi, G.M., 2001. The altitude effect on the isotopic composition of tropical rains. Chem. Geol. 181:147–167. https://doi.org/10.1016/S0009-2541(01)00279-0.

Harwood, K.G., Gillon, J.S., Griffiths, H., Broadmeadow, M.S.J., 1998. Diurnal variation of $D^{13}CO_2$, $D.C.^{18}O^{16}O$ and evaporative site enrichment of $dH_n^{18}O$ in *Piper aduncum* under field conditions in Trinidad. Plant Cell Environ. 21, 269–283.

Hassen, A., Talore, D.G., Tesfamariam, E.H., Friend, M.A., Mpanza, T.D.E., 2017. Potential use of forage-legume intercropping technologies to adapt to climate-change impacts on mixed crop-livestock systems in Africa: a review. Reg. Environ. Chang. 73 (10). https://doi.org/10.1007/s10113-017-1131-7.

Hemp, A., 2009. Climate change and its impact on the forests of Kilimanjaro. Afr. J. Ecol. 47:3–10. https://doi.org/10.1111/j.1365-2028.2008.01043.x.

Hijmans, R.J., Cameron, S.E., Parra, J.L., Jones, P.G., Jarvis, A., 2004. The WorldClim Interpolated Global Terrestrial Climate Surfaces. Available at. http://biogeo.berkeley.edu/, version 1.3.

Hughes, C.E., Crawford, J., 2012. A new precipitation weighted method for determining the meteoric water line for hydrological applications demonstrated using Australian and global GNIP data. J. Hydrol. 464–465:344–351. https://doi.org/10.1016/j.jhydrol.2012.07.029.

IAEA, 1992. Statistical Treatment of Data on Environmental Isotopes in Precipitation. Technical Report Series 331IAEA, Vienna (781 pp).

IAEA/WMO, 2017. Global Network of Isotopes in Precipitation. The GNIP Database. Available at. http://www.iaea.org/water.

IPCC, 2014. Summary for policymakers. In: Climate change 2014: Impacts, adaptation, and vulnerability. In: Field, C.B., Barros, V.R., Dokken, D.J., Mach, K.J., Mastrandrea, M.D., Bilir, T.E., Chatterjee, M., Ebi, Y.L., Estrada, Y.O., Genova, R.C., Girma, B., Kissel, E.S., Levy, A.N., MacCracken, S., Mastrandrea, P.R., White, L.L. (Eds.), Part A: Global and Sectoral Aspects. Contribution of Working Group II to the Fifth Assessment Report of the Intergovermental Panel on Climate Change. Cambridge University Press, Cambridge, UK and New York, USA, pp. 1–32.

ISCGM (International Steering Committee for Global Mapping), GSI (Geospatial Information Authority of Japan), Chiba University and collaborating organizations, 2008. Vegetation (Percent Tree Cover) - Global version - Version 2. https://globalmaps.github.io/ptc.html, Accessed date: July 2017.

IUCN and UNEP-WCMC, 2015. The World Database on Protected Areas (WDPA) UNEP-WCMC. Cambridge, UK Available at. www.protectedplanet.net, Accessed date: July 2017.

Jasechko, S., Sharp, Z.D., Gibson, J.J., Birks, S.J., Yi, Y., Fawcett, P.J., 2013. Terrestrial water fluxes dominated by transpiration. Nature 496, 347–350.

Johnsen, S.J., Dansgaard, W., White, J.W.C., 1989. The origin of Arctic precipitation under present and glacial conditions. Tellus B 41, 452–468.

Kelemen, Z., Gillikin, D.P., Graniero, L.E., Havel, H., Darchambeau, F., Borges, A.V., Yambélé, A., Bassirou, A., Bouillon, S., 2017. Calibration of hydroclimate proxies in freshwater bivalve shells from Central and West Africa. Geochim. Cosmochim. Acta 208:41–62. https://doi.org/10.1016/j.gca.2017.03.025.

Kidd, C.A., 1983. Water Resources Evaluation of Lake Malawi and the Shire River. World Meteological Organization, Geneva.

Kobayashi, S., Matricardi, M., Dee, D.P., Uppala, S., 2009. Toward a consistent reanalysis of the upper stratosphere based on radiance measurements from SSU and AMSU-A. Q. J. R. Meteorol. Soc. 135:2086–2099. https://doi.org/10.1002/qj.514.

Kolding, J., Medard, M., Mkumbo, O., van Zwieten, P., 2014. Status, trends and management of the Lake Victoria Fisheries. In: Welcomme, R., Valbo-Jorgensen, J., Halls, A. (Eds.), Inland Fisheries Evolution: Case Studies from four Continents. Food and Agriculture Organisation of the United Nations, Rome, Italy, pp. 49–62.

Kotir, J.H., 2011. Climate change and variability in sub-Saharan Africa: a review of current and future trends and impacts on agriculture and food security. Environ. Dev. Sustain. 13:587–605. https://doi.org/10.1007/s10668-010-9278-0.

Lehner, B., Döll, P., 2004. Development and validation of a global database of lakes, reservoirs and wetlands. J. Hydrol. 296 (1–4), 1–22.

Lehner, B., Verdin, K., Jarvis, A., 2006. HydroSHEDS Technical Documentation. World Wildlife Fund, Washington, D. C Available at. http://hydrosheds.cr.usgs.gov.

Levin, N.E., Zipser, E.J., Cerling, T.E., 2009. Isotopic composition of waters from Ethiopia and Kenya: insights into moisture sources for eastern Africa. J. Geophys. Res. 114, D23306. https://doi.org/10.1029/2009JD012166.

Lindsay, C.S., Dyer, J.C., Reed, M.S., Dougill, A.J., Twyman, C., Mkwambisi, D., 2009. Adaptations to climate change, drought and desertification: local insights to enhance policy in southern Africa. Environ. Sci. Pol. 12:748–765. https://doi.org/10.1016/j.envsci.2009.04.002.

Liotta, M., Brusca, L., Grassa, F., Inguaggiato, S., Longo, M., Madonia, P., 2006a. Geochemistry of rainfall at Stromboli volcano (Aeolian Islands): isotopic composition and plume-rain interaction. Geochem. Geophys. Geosyst. 7 (7). https://doi.org/10.1029/2006GC001288.

Liotta, M., Favara, R., Valenza, M., 2006b. Isotopic composition of the precipitations in the central Mediterranean: origin marks and orographic precipitation effects. J. Geophys. Res. 111, D19302. https://doi.org/10.1029/2005JD006818.

Liotta, M., Grassa, F., D'Alessandro, W., Favara, R., Candela, E.G., Pisciotta, A., Scaletta, C., 2013. Isotopic composition of precipitation and groundwater in Sicily, Italy. Appl. Geochem. 34:199–206. https://doi.org/10.1016/j.apgeochem.2013.03.012.

Lobell, D.B., Burke, M.B., Tebaldi, C., Mastrandrea, M.D., Falcon, W.P., Naylor, R.L., 2008. Prioritizing climate change adaptation needs for food security in 2030. Science 319: 607–610. https://doi.org/10.1126/science.1152339.

Lyon, B., DeWitt, D.G., 2012. A recent and abrupt decline in the East African long rains. Geophys. Res. Lett. 39, L02702. https://doi.org/10.1029/2011GL050337.

Lyons, R.P., Kroll, C.N., Scholz, C.A., 2011. An energy-balance hydrologic model for the Lake Malawi Rift Basin, East Africa. Glob. Planet. Chang. 75, 83–97.

Mahmood, R., Pielke, R.A., Hubbard, K.G., Niyogi, D., Dirmeyer, P.A., McAlpine, C., Carleton, A.M., Hale, R., Gameda, S., Beltrán-Przekurat, A., Baker, B., McNider, R., Legates, D.R., Shepherd, M., Du, J., Blanken, P.D., Frauenfeld, O.W., Nair, U.S., Fall, S., 2014. Land cover changes and their biogeophysical effects on climate. Int. J. Climatol. 34: 929–953. https://doi.org/10.1002/joc.3736.

Mandeville, A.N., Batchelor, C., 1990. Estimation of Evapo-Transpiration in Malawi. Report 110. Institute of Hydrology, London.

Mduma, N.P., Komakech, H.C., Zhang, J., Muzuka, A.N.N., 2016. Application of isotopes and water balance on Lake Duluti–groundwater interaction, Arusha, Tanzania of isotopes and water balance on lake duluti-groundwater interaction, Arusha, Tanzania. Hydrol. Earth Syst. Sci. Discuss. https://doi.org/10.5194/hess-2016-176.

Mendelsohn, R., 2008. The impact of climate change on agriculture in developing countries. J. Nat. Resour. Policy Res. 1:5–19. https://doi.org/10.1080/19390450802495882.

Merlivat, L., Jouzel, J., 1979. Global climatic interpretation of the deuterium-oxygen 18 relationship for precipitation. J. Geophys. Res. 84, 5029–5033.

Moser, H., Stichler, W., 1971. Deuterium and oxygen-18 contents as an index of the properties of snow covers. Snow Mechanics Symposium, Proc. Grindelwald Symp. 114, pp. 122–135.

Müller, C., Waha, K., Bondeau, A., Heinke, J., 2014. Hotspots of climate change impacts in sub-Saharan Africa and implications for adaptation and development. Glob. Chang. Biol. 20:2505–2517. https://doi.org/10.1111/gcb.12586.

Munyaneza, O., Wenninger, J., Uhlenbrook, S., 2012. Identification of runoff generation processes using hydrometric and tracer methods in a meso-scale catchment in Rwanda. Hydrol. Earth Syst. Sci. 16 (7):1991–2004. https://doi.org/10.5194/hess-16-1991-2012.

Mutiibwa, D., Kilic, A., Irmak, S., 2014. The effect of land cover/land use changes on the regional climate of the USA high plains. Climate 2:153–167. https://doi.org/10.3390/cli2030153.

Muvundja, A.F., Wüest, A., Isumbisho, M., Kaningini, M., Pasche, N., Rinta, P., Schmid, M., 2014. Modelling Lake Kivu water level variations over the last seven decades. Limnol. Ecol. Manag. Inland Water 47:21–33. https://doi.org/10.1016/j.limno.2014.02.003.

Niang, I., Ruppel, O.C., Abdrabo, M.A., Essel, A., Lennard, C., Padgham, J., Urquhart, P., 2014. Africa. Climate Change 2014: Impacts, Adaptation and Vulnerability. Contribution of Working Group II to the Fifth Assessment Report of the Intergovernmental Panel on Climate Change. Cambridge University Press, Cambridge.

Nicholson, S.E., 1996. A review of climate dynamics and climate variability in eastern Africa. In: Johnson, T.C., Odada, E.O. (Eds.), The Limnology, Climatology and Paleoclimatology of the East African Lakes. Gordon and Breach, Amsterdam, pp. 25–56.

Nicholson, S., Yin, X., 2001. Rainfall condition in equatorial East Africa during the nineteenth century as inferred from the record of lake Victoria. Climate Change 48, 387–398.

Njitchoua, R., Sigha-Nkamdjou, L., Dever, L., Marlin, C., Sighomnou, D., Nia, P., 1999. Variations of the stable isotopic compositions of rainfall events from the Cameroon rain forest, Central Africa. J. Hydrol. 223, 17–26.

Nsubuga, F.N.W., Namutebi, E.N., Nsubuga-Ssenfuma, M., 2014. Water resources of Uganda: an assessment and review. J. Water Resour. Prot 6, 1297–1315.

Odada, E., 2001. Stable isotopic composition of east African lake waters. In: Gourcy, L. (Ed.), Use of Isotope Techniques in Lake Dynamics Investigations. IAEA, Vienna, pp. 43–48.

Patz, J.A., Campbell-Lendrum, D., Holloway, T., Foley, J.A., 2005. Impact of regional climate change on human health. Nature 438:310–317. https://doi.org/10.1038/nature04188.

Pereira, R., Bovolo, C.I., Forsythe, N., Pedentchouk, N., Parkin, G., Wagner, T., 2014. Seasonal patterns of rainfall and river isotopic chemistry in northern Amazonia (Guyana): from the headwater to the regional scale. J. S. Am. Earth Sci. 52:108–118. https://doi.org/10.1016/j.jsames.2014.02.005.

Pfahl, S., Sodemann, H., 2014. What controls deuterium excess in global precipitation? Clim. Past 10:771–781. https://doi.org/10.5194/cp-10-771-2014.

Pfahl, S., Wernli, H., 2008. Air parcel trajectory analysis of stable isotopes in water vapor in the eastern Mediterranean. J. Geophys. Res. 113, D20104. https://doi.org/10.1029/2008JD009839.

Piao, S., Ciais, P., Huang, Y., Shen, Z., Peng, S., Li, J., Zhou, L., Liu, H., Ma, Y., Ding, Y., Friedlingstein, P., Liu, C., Tan, K., Yu, Y., Zhang, T., Fang, J., 2010. The impacts of climate change on water resources and agriculture in China. Nature 467:43–51. https://doi.org/10.1038/nature09364.

Pielke, R.A., Adegoke, J., Beltran-Przekurat, A., Hiemstra, J.L., Nair, U.S., Niyogi, D., Nobis, T. E., 2007. An overview of regional land-use and land-cover impacts on rainfall. Tellus B 59:587–601. https://doi.org/10.1111/j.1600-0889.2007.00251.x.

Putman, A.L., Feng, X., Sonder, L.J., Posmentier, E.S., 2017. Annual variation in event-scale precipitation δ^2H at Barrow, AK, reflects vapor source region. Atmos. Chem. Phys. 17: 4627–4639. https://doi.org/10.5194/acp-17-4627-2017.

Reich, P.F., Numbem, S.T., Almaraz, R.A., Eswaran, H., 2001. Land resource stresses and desertification in Africa. In: Bridges, E.M., Hannam, I.D., Oldeman, L.R., Pening de Vries, F. W.T., Scherr, S.J., Sompatpanit, S. (Eds.), Responses to Land Degradation. Proc. 2nd. International Conference on Land Degradation and Desertification, Khon Kaen, Thailand. Oxford Press, New Delhi, India.

Rolph, G., Stein, A., Stunder, B., 2017. Real-time environmental applications and display sYstem: READY. Environ. Model. Softw. 95:210–228. https://doi.org/10.1016/j.envsoft.2017.06.025.

Rozanski, K., Araguaś-Araguaś, L., Gonfiantini, R., 1993. Isotopic patterns in modern global precipitation. In: Swart, P.K., Lohmann, K.C., Mckenzie, J., Savin, S. (Eds.), Climate Change in Continental Isotopic Records. 78. American Geophysical Union:pp. 1–35. https://doi.org/10.1029/GM078p0001.

Russell, J.M., Johnson, T.C., 2006. The water balance and stable isotope hydrology of Lake Edward, Uganda-Congo. J. Great Lakes Res. 32:77–90. https://doi.org/10.3394/03801330(2006)32[77:TWBASI]2.0.CO;2.

Serdeczny, O., Adams, S., Baarsch, F., Coumou, D., Robinson, A., Hare, W., Schaeffer, M., Perrette, M., Reinhardt, J., 2016. Climate change impacts in Sub-Saharan Africa from physical changes to their social repercussions. Reg. Environ. Chang. https://doi.org/10.1007/S10113-015-0910-2.

Seto, C.K., Guneralp, B., Hutyra, R.L., 2012. Global forecasts of urban expansion to 2030 and direct impacts on biodiversity and carbon pools. PNAS 109, 16083–16088.

Shahin, M., 2013. Hydrology and water resources of Africa. Water Sci. Technol. Lib. 41 (Netherlands).

Simmons, A.J., Willett, K.M., Jones, P.D., Thorne, P.W., Dee, D.P., 2010. Low-frequency variations in surface atmospheric humidity, temperature and precipitation: inferences from reanalyses and monthly gridded observational datasets. J. Geophys. Res. 115, D01110. https://doi.org/10.1029/2009JD012442.

Singh, R.B., Shi, C., 2014. Advances in observation and estimation of land use impacts on climate changes: improved data, upgraded models, and case studies. Adv. Meteorol. 2014:1–7. https://doi.org/10.1155/2014/748169.

Slingo, J., Spencer, H., Hoskins, B., Berrisford, P., Black, E., 2005. The meteorology of the western Indian Ocean, and the influence of the East African highlands. Phil. Trans. R. Soc. A 363:25–42. https://doi.org/10.1098/rsta.2004.1473.

Stein, A.F., Draxler, R.R., Rolph, G.D., Stunder, B.J.B., Cohen, M.D., Ngan, F., 2015. NOAA's HYSPLIT atmospheric transport and dispersion modeling system. Bull. Am. Meteorol. Soc. 96:2059–2077. https://doi.org/10.1175/BAMS-D-14-00110.1.

Stewart, M.K., 1975. Stable isotope fractionation due to evaporation and isotopic-exchange of falling water drops: applications to atmospheric processes and evaporation of lakes. J. Geophys. Res. 80, 1133–1146.

Sultan, B., Gaetani, M., 2016. Agriculture in West Africa in the twenty-first century: climate change and impacts scenarios, and potential for adaptation. Front. Plant Sci. 7: 1262. https://doi.org/10.3389/fpls.2016.01262.

Swenson, S., Wahr, J., 2009. Monitoring the water balance of Lake Victoria, East Africa, from space. J. Hydrol. 370 (1–4), 163–176.

Tabbo, A.M., Amadou, Z., Danbaky, A.B., 2016. Evaluating farmers adaptation strategies to climate change: a case study of Kaou local government area, Tahoua State, Niger Republic. Jamba J. Disast. Risk Stud. 8:1–5. https://doi.org/10.4102/jamba.v8i3.241.

Taylor, R.G., Mileham, L., Tindimugaya, C., Majugu, A., Muwanga, A., Nakilez, B., 2006. Recent glacial recession in the Rwenzori mountains of East Africa due to rising air temperature. Geophys. Res. Lett. 33, L10402.

Thiery, W., Davin, E., Panitz, H., Demuzere, M., Lhermitte, S., Van Lipzig, N., 2015. The impact of the African Great Lakes on the regional climate. J. Clim. 28:4061–4085. https://doi.org/10.1175/JCLI-D-14-00565.1.

Tierney, J.E., Smerdon, J.E., Anchukaitis, K.J., Seager, R., 2013. Multidecadal variability in East African hydroclimate controlled by the Indian Ocean. Nature 493:389–392. https://doi.org/10.1038/nature11785.

Trabucco, A., Zomer, R.J., 2009. Global Aridity Index (Global-Aridity) and Global Potential Evapotranspiration (Global-PET) Geospatial Database. CGIAR Consortium for Spatial Information. (Published online, available from the CGIAR-CSI GeoPortal at). http://www.csi.cgiar.org.

Trabucco, A., Zomer, R.J., Bossio, D.A., van Straaten, O., Verchot, L.V., 2008. Climate change mitigation through afforestation/reforestation: a global analysis of hydrologic impacts with four case studies. Agric. Ecosyst. Environ. 126, 81–97.

Ummenhofer, C.C., Gupta, A.S., England, M.H., Reason, C.J.C., 2009. Contributions of Indian Ocean sea surface temperatures to enhanced East African rainfall. J. Clim. 22, 993–1013.

UNPD (United Nations, Department of Economic and Social Affairs, Population Division), 2015. Population 2030: Demographic challenges and opportunities for sustainable development planning (ST/ESA/SER.A/389).

Verburg, P., Hecky, E.H., 2003. Wind patterns, evaporation, and related physical variables in Lake Tanganyika, East Africa. J. Great Lakes Res. 29, 48–61.

Verburg, P., Hecky, R.E., Kling, H., 2003. Ecological consequences of a century of warming in Lake Tanganyika. Science 3001, 505–507.

Wang, L., Good, S., Caylor, K., Cernusak, L.A., 2012. Direct quantification of leaf transpiration isotopic composition. Agric. For. Meteorol. 154–155, 127–135.

Wang, X., Edwards, R.L., Auler, A.S., Cheng, H., Kong, X., Wang, Y., Cruz, F.W., Dorale, J.A., Chiang, H.-W., 2017. Hydroclimate changes across the Amazon lowlands over the past 45,000 years. Nature 541:204–207. https://doi.org/10.1038/nature20787.

Wassenaar, L.I., Coplen, T., B and Pradeep K. A., 2014. Approaches for achieving long-term accuracy and precision of δ^{18}O and δ^2H for waters analyzed using laser absorption spectrometers. Sci. Technol. 48:1123–1131. https://doi.org/10.1021/es403354n.

Windhorst, D., Waltz, T., Timbe, E., Frede, H.-G., Breuer, L., 2013. Impact of elevation and weather patterns on the isotopic composition of precipitation in a tropical montane rainforest. Hydrol. Earth Syst. Sci. 17:409–419. https://doi.org/10.5194/hess-17-409-2013.

Wirmvem, M.J., Ohba, T., Kamtchueng, B.T., Taylor, E.T., Fantong, W.Y., Ako, A.A., 2016. Variation in stable isotope ratios of monthly rainfall in the Douala and Yaounde cities, Cameroon: local meteoric lines and relationship to regional precipitation cycle. Appl Water Sci:1–14 https://doi.org/10.1007/s13201-016-0413-4.

Yin, X., Nicholson, S.E., 1998. The water balance of Lake Victoria. Hydrol. Sci. J. Sci. Hydrol. 43 (5), 789–811.

Zandbergen, P., 2008. Applications of shuttle radar topography mission elevation data. Geogr. Compass. 2, 1404–1431.
Zeng, N., Neelin, J.D., Lau, K.-M., Tucker, C.J., 1999. Enhancement of interdecadal climate variability in the Sahel by vegetation interaction. Science 286 (5444), 1537–1540.
Zhang, L., Nan, Z., Yu, W., Ge, Y., 2015. Modeling land-use and land-cover change and hydrological responses under consistent climate change scenarios in the Heihe River Basin, China. Water Resour. Manag. 29:4701–4717. https://doi.org/10.1007/s11269-015-1085-9.
Zomer, R.J., Bossio, D.A., Trabucco, A., Yuanjie, L., Gupta, D.C., Singh, V.P., 2007. Trees and Water: Smallholder Agroforestry on Irrigated Lands in Northern India. International Water Management Institute, Colombo, Sri Lanka, p. 45 (IWMI Research Report 122).
Zomer, R.J., Trabucco, A., Bossio, D.A., van Straaten, O., Verchot, L.V., 2008. Climate change mitigation: a spatial analysis of global land suitability for clean development mechanism afforestation and reforestation. Agric. Ecosyst. Environ. 126, 67–80.